STRASBOURG

CRN/PN - 87/06

Search for Correlations between Prolate-Shape Collective and Oblate-Shape Non-Collective Nuclear Rotation : High Spin States in ^{159,160}Yb

Th.BYRSKI, F.A.BECK, J.C.MERDINGER and A.NOURREDDINE.

Centre de Recherches Nucléaires, F-67037 Strasbourg Cedex, France

H.W.CRANMER-GORDON, D.V.ELENKOV, P.D.FORSYTH, D.HOWE, M.A.RILEY,

and J.F.SHARPEY-SCHAFER

Oliver Lodge Laboratory, The University of Liverpool,

Liverpool L69 3BX, U.K.

J.SIMPSON

Daresbury Laboratory, Daresbury, Warrington WA4 4AD, UK.

and

J.DUDEK and W.NAZAREWICZ

Centre de Recherches Nucléaires et Université Louis Pasteur,

F-67037 Strasbourg Cedex, France

CENTRE DE RECHERCHES NUCLEAIRES

STRASBOURG

IN2P3 CNRS

UNIVERSITE LOUIS PASTEUR

Search for Correlations between Prolate-Shape Collective and Oblate-Shape Non-Collective Nuclear Rotation : High Spin States in ^{159,160}Yb

T.BYRSKI, F.A.BECK, J.C.MERDINGER and A.NOURREDDINE.

Centre de Recherches Nucléaires, F-67037 Strasbourg Cedex, France.

H.W.CRANMER-GORDON, D.V.ELENKOV*, P.D.FORSYTH, D.HOWE, M.A.RILEY†** and J.F.SHARPEY-SCHAFER

Oliver Lodge Laboratory, The University of Liverpool,

Liverpool L69 3BX,U.K.

J.SIMPSON

Daresbury Laboratory, Daresbury, Warrington WA4 4AD, UK.

and

J.DUDEK and W.NAZAREWICZ**

Centre de Recherches Nucléaires et Université Louis Pasteur,

F-67037 Strasbourg Cedex, France

* Institute of Nuclear Research and Nuclear Energy 1184 - Sofia, Bulgaria

** and The Niels Bohr Institute, Blegdamsvej 17, 2200 Copenhagen, Denmark

Abstract

High-spin states of ^{159,160}Yb have been studied using the escape-suppressed array TESSA 2. Extensions of yrast and lateral bands have been found up to $I \sim 40$. Experimental data suggest strong correlations between maximum alignment configurations of the valence nucleons and related collective states. Theoretical analysis fully supports the idea of prolate-collective vs. oblate-non-collective correlations. Band termination interpretation is discussed.

I. Introduction

It has been more than a decade during which numerous high-spin studies have focused on individual/nucleon alignment and the related band crossing phenomena. It has been found that the accompanying rearrangement in the quasiparticle structure of the yrast state wave functions often manifests itself dramatically, as a back-bending or an up-bending pattern. Making an analysis based entirely on the nuclear decay schemes it has been possible to extract the characteristic crossing frequencies and obtain a systematic quasiparticle interpretation for yrast and lateral bands for many nuclei. At present a fairly consistent picture of the individual quasiparticle structure of the majority of known rotational nuclei exists.

The shape evolution effects are collective in nature and much more difficult to establish from the decay schemes alone. An expectation that the smooth $E(I) \sim I(I + 1)$ pattern breaking into an irregular pattern necessarily demonstrates the prolate-to-oblate shape transition is not entirely correct. Indeed theoretical calculations indicate that when progressive alignment forces the shape evolution from prolate-collective to oblate-non-collective configurations, there may be several bands (corresponding to some distinct triaxial configurations) crossing each other in a relatively narrow spin range. As a result the yrast sequence may become irregular-looking and an additional criterion, for instance the life-time or Doppler shift measurement help distinguishing between slightly irregular-collective and irregular non-collective decay schemes.

The shape evolution from prolate-collective to oblate-non-collective rotational pattern has been predicted theoretically[1] and the calculations [2-5]

which followed*) pointed to the N ∿ 90 isotones as the most favourable cases in the rare earth nuclei. Various theoretical approaches may differ in estimating the spin range in which the shape transition is most likely to occur. Using the combined approach of the recent studies[5] we arrive at the result illustrated in Fig.1 for the six even-even ytterbium nuclei ($^{158}_{70}Yb_{88}$ to $^{168}_{70}Yb_{98}$). In the lowest temperature limit the N ≥ 90 isotopes are expected to rotate collectively in the yrast states at least up to I ∿ 30. However the nucleus ^{160}Yb is predicted to reveal a shape coexistence between the prolate-collective and oblate non-collective configurations whose excitation energies become comparable above I ∿ 36. This shape coexistence has an important influence on the high-spin behaviour as will be discussed later. At I ∿ 30 the nucleus $^{158}_{70}Yb_{88}$ is expected to be well on its way towards a totally aligned yrast sequence corresponding to configurations at oblate shape. The latter nucleus has been a subject of recent experimental studies[7] (see also the related theoretical interpretation in Ref.[8]).

The present study focuses on the high-spin properties of $^{159,160}Yb$ nuclei which fall precisely into the expected shape transition area.

By studying the ^{160}Yb nucleus for the first time with an escape-suppressed array we expected to extend the knowledge of its yrast line well above the first proton ($\pi h_{11/2}$) alignment (at $I^{\pi} = 26^{+}$) and possibly find evidence for a shape transition. Recent experimental results[9] for the isotone $^{158}_{68}Er_{90}$ have already been interpreted in terms of prolate to oblate shape transition. Moreover, we hoped to examine the non-yrast side band structures which are expected to experience alignment and deformation driving forces similar to those ruling the behaviour of the yrast states. In fact the ^{160}Yb

---

*) In this study we concentrate on a few selected ytterbium nuclei and the quotation of references has been limited. More general bibliography can be found e.g. in Refs.5,6).

nucleus has been examined from various points of view and several experimental and theoretical studies have been devoted entirely or in a big part to analysing its rotational properties. In particular after finding[10] an onset of the second backbending in the yrast line and in some excited bands[11] the "moderately" high-spin structure of ^{160}Yb has been undestood[11,12] in terms of quasiparticle excitations and alignment properties. Our study adds several new transitions in the yrast and side bands extending the identified transitions up to an I $\sim$ 40 limit.

We investigate also the ^{159}Yb nucleus in which the yrast line has been assigned to the $\nu i_{13/2}$ configuration by analogy to all odd-N nuclei in this region. Preliminary results for this nucleus by Courtney et al., can be found in ref.[13].

In the theoretical interpretation we examine in detail the deviations from the strict I(I+1)-rule found in our results for frequencies ω above the alignment frequency of the first proton pair. In particular such deviations are expected to be present when the effect of band termination is about to take place. Our calculations support the band termination picture but reveal also further correlations. It has already been noticed[14] that the strongest deviations from the I(I +1)-rule occur at I $\sim$ (30 to 40) in some collectively rotating N $\sim$ 90 nuclei. This takes place for the spin values which coincide with the spins of the maximum alignment configurations in the oblate shape (non-collective) states. Our analysis suggests that the correlation between prolate-shape collective and the oblate shape non collective states appears over longer stretches of the yrast line and lateral bands and applies also to non-optimal configurations.

II. Experimental Method.

The experiment was carried out using the 20 MV tandem Van de Graaff accelerator (Nuclear Structure Facility or N.S.F.) at the Daresbury Laboratory, U.K. The reactions were $^{120}Sn(^{44}Ca,5n)^{159}Yb$ and $^{120}Sn(^{44}Ca,4n)^{160}Yb$ studied simultaneously at a beam energy of 210 MeV. The target consisted of five stacked 300 mg/cm^{-2} foils of ^{120}Sn giving a total thickness of 1.5 mg cm^{-2}. The beam current was between 5 and 8 particle nanoamperes. Gamma-rays were detected in the spectrometer TESSA2 which consists of six Ge detectors at angles of $\pm$ 30°, $\pm$ 90° and $\pm$ 150° to the beam direction in NaI escape suppression shields outside a 50 element bismuth germinate (BGO) crystal ball[15]. The crystal ball gave information on the total energy in a γ-ray cascade and on the number of γ-rays emitted. Events were selected in which two escape suppressed Ge detectors are in coincidence with at least one BGO detector.

The information from the BGO crystal ball can be used to enhance the information in a given reaction channel. In Fig. 2 plots are shown of the total energy (ΣE_γ) deposited in the BGO ball against the number of elements (fold) which have detected a photon. These data have been selected, by gating on known strong peaks in the Ge spectra, to be either in the 5n channel (^{159}Yb, Fig. 2a) or to be in the 4n channel (^{160}Yb, Fig. 2b). When analysing the coincidence data between Ge escape suppressed spectrometers, gates were set on the BGO crystal ball data, to select the appropriate channel and to reduce the contribution of the other channel as much as possible.

As the six Ge detectors in the γ-ray spectrometer are at $\pm$ 30°, $\pm$ 90° and $\pm$ 150° the gains of the spectra at $\pm$ 30° and $\pm$ 150° have to be corrected for the full Doppler shift due to the motion of the freely recoiling residual nucleus. This correction procedure is done numerically knowing the calibration

of each spectrum rather than by adjusting the gains of each amplifier.

The different angles of the Ge detectors may be used to obtain angular correlation data giving an indication of the multipolarity of transitions. This has been done by gating on known E2 transitions at lower spins in the nucleus, observed only in the $\pm$ 30° and $\pm$ 150° (= 180° - 30°) detectors, and separating the photons in coincidence with these into two spectra, one from the $\pm$ 90° detectors and the other from the remaining 30° or 150° detectors. The ratio W(30)/W(90) can be then formed for any γ-ray peak. For stretched quadrupole radiation this ratio is expected to be a factor of two larger than for pure stretched dipole radiation. The angular correlation ratio was normalised to 1 for the average value of previously known stretched E2 transitions. Stretched quadrupole transitions are assumed to be E2. Spin and parity assignments are made on the basis of previous work, on the W(30)/W(90) ratios plus arguments from the systematic behaviour of known band structure in neighbouring nuclei.

III. Results for ^{159}Yb

In this section the experimental results for ^{159}Yb are given and their interpretation is discussed.

IIIa. Experimental results

The decay scheme we have deduced for ^{159}Yb is shown in Fig.3. The lowest state at $I^{\pi} = 13/2^{+}$ is not the ground state, its excitation energy is not known but we take its energy as zero for reference purposes.

We observe the yrast band up to $65/2^{+}$. A spectrum of γ-rays in coincidence with the 748, 790 and 774 keV transitions is shown in Fig.4a. The ordering of the transitions has been decided by examining in detail the relative intensities of the γ-rays in all the spectra gated by transitions in this band (see for example the spectrum in coincidence with the 774 keV γ-ray shown in Fig.4b).

The lowest negative parity band is expected, on the basis of experimental systematics and also the theoretical calculations, to have positive signature, cf. also Sec.IIIb. Our data connects the previously observed sideband γ-rays to the yrast states as shown in the decay scheme in Fig.3. A relatively simple example of these connecting decays is illustrated in Fig.4c which is a spectrum of the γ-rays in coincidence with the 481 keV transition decay from the $29/2^-$ to the $25/2^-$ level. Figure 4d shows in the same band a spectrum in coincidence with the 714 keV transition decay from the $45/2^-$ to the $41/2^-$ level. In Fig.4e γ-rays in coincidence with the 811 keV transition show the decay of the third band. A sequence of 11 transitions starting from 534 keV up to 931 keV is observed in coincidence. The 606 and 769 keV, transitions which connect this sequence with the yrast band have angular correlation characteristics of pure stretched dipole radiation. We therefore take this band to have negative signature starting with a $31/2^-$ state at 2700 keV and extending to a $71/2^-$ level at 10381 keV. A 950 keV γ-ray is tentatively assigned as the $75/2^- \rightarrow 71/2^-$ transition.

The spin assignments given in the decay scheme shown in figure 3 are consistent with the measured W(30)/W(90) ratios which are plotted against γ-ray energy (E_γ) in Figure 5. It can be seen from the figure that the ratio observed for all known stretched E2 transitions is near to unity which is also the case for the transitions that we have assigned as in-band. The 365, 606 and 769 keV transitions are all consistent with being pure stretched dipole (E1) transitions, the 260 keV transition should be a stretched M1 but would require some E2 admixture to reproduce the correlation data.

The high spin level structure of ^{159}Yb has also been studied by Courtney et al.[13]. Several differences exist between the results given in these two reports and therefore we will restrict our comments to the latest reported level scheme from Courtney et al. The latter level scheme is in very close agreement with that of the present work. They observe the same sequence of

transitions up to the $65/2^+$ level in the (+,1/2) band, but with an extra tentative transition of 1098 keV as the next inband decay. The (-,-1/2) sequence is also followed up to spin $71/2^-$ in agreement with our results. For the (-,1/2) sequence there is agreement up to spin $69/2^-$ except that Courtney et al reverse the ordering of the 785 keV ($57/2^- \rightarrow 53/2^-$) and the 798 keV ($53/2^- \rightarrow 49/2^-$) transitions. We do not consider this small disagreement as very serious and feel that with the present available data no clear choice can be made between either of these two possibilities. Since these transitions are very close in energy no significant change in the physical behaviour of this band results if the 798 and 785 keV transitions were to be interchanged in the level scheme. At the top of this band Courtney et al. observe a 1016 keV ($73/2^- \rightarrow 69/2^-$) transition with a tentative 1064 keV ($77/2^- \rightarrow 73/2^-$) transition above it. In the (+,-1/2) sequence they observe an additional level at 2185 keV.

IIIb. Interpretation of the experimental results and discussion

We begin with a brief analysis of the single particle properties of ^{159}Yb and the related quasiparticle excitation scheme. This scheme underlies the characteristic features of the entire decay pattern observed and helps in their microscopic understanding.

In calculating both single-particle and quasiparticle wave functions the deformed Woods-Saxon potential has been used. We calculated first the equilibrium deformation ($\beta_2 = 0.215$, $\gamma = 0°$, $\beta_4 = 0.02$) using the Strutinsky method. At the above deformation the strongly alignment-susceptible $i_{13/2,K=1/2}$ orbital appears closest to the Fermi level, λ_N, thus giving rise to the $K = 1/2$ ground state decoupled band. We have calculated the corresponding decoupling parameter value with the result $a = 6.523$. For an axial nucleus with the other possible couplings neglected, the low spin part of the decoupled band is approximately expressed by

$$E_{K=1/2}(I) = \frac{\hbar^2}{2J}\{I(I+1) + a(-1)^{I+1/2}(I+\tfrac{1}{2})\}$$

It then follows that the band-head of the positive parity band should have $(I^\pi,K) = (5/2^+,1/2)$.

Figure 6a gives a few lowest energy quasiparticle excitations and illustrates the quasiparticle evolution with rotational frequency ω. The lowest $i_{13/2}$ quasi particle routhian (originating from the $i_{13/2,K=1/2}$ level) situated about 300 keV above λ_N at $\omega = 0$ approaches the Fermi energy with increasing rotational frequency due to progressing alignment. This causes a crossing in terms of quasiparticles at $\hbar\omega_{cr} \approx 0.23$ MeV. However, in the odd particle system $N = 89$ such a crossing causes no influence on the observed band properties due to the well known effect of blocking. From the quasiparticle diagram of Fig.6a

two further features of the decay scheme of ^{159}Yb can be understood. First, the yrast line should, for $\hbar\omega \geq 0.3$ MeV, have negative parity with the signature $\alpha = 1/2$. This is because soon after the first crossing the positive parity quasiparticle energies grow quickly with ω while the two negative parity states originating from the $\nu h_{9/2,K=3/2}$ orbital slope gradually down. This expectation is in full agreement with the experimental findings, see Fig.3, where between spin $41/2^-$ and $45/2^-$ the negative parity, $\alpha = + 1/2$, sequence crosses the positive parity band and becomes yrast. Similarly the $\alpha = - 1/2$ negative parity sequence crosses the positive parity band between spin $55/2^-$ and $59/2^-$. These crossings correspond well with the theoretical predictions of crossings at $\hbar\omega = 0.33$ MeV and 0.37 MeV, respectively, see fig.6a.

Two levels at 1064 and 1612 keV connected by a 548 keV transition were observed. These levels are assigned, from angular correlation measurements, spins of 19/2 and 23/2, respectively. We interpret these levels as members of the unfavoured $i_{13/2}$ band, and therefore they are tentatively assigned as positive parity. For rotational frequencies $\hbar\omega \geq 0.3$ MeV this sequence should have an excitation energy above the yrast as big as $\sim$ 800 to 1200 keV, cf. Fig.6a. This behaviour explains why the corresponding band is not observed at higher spins.

The proton alignment is experienced by all the observed bands at approximately equal frequencies $\hbar\omega^p_{cr} \approx 0.4$ MeV slightly smaller than the corresponding ^{160}Yb proton crossing frequency. The calculated quadrupole deformations for ^{159}Yb evolve from typically $\beta_2 = 0.22$ at the ground state to $\beta_2 = 0.18$ at $I \sim 61/2$. The corresponding deformations for ^{160}Yb remain larger by an amount $\Delta\beta_2 \approx 0.03$ and this difference causes the observed lowering of the proton crossing frequency in ^{159}Yb as compared to ^{160}Yb (for discussion of the deformation dependence of $\hbar\omega^p_{cr}$ see e.g. ref.[18]). The proton quasiparticle spectrum is illustrated in Fig.6b analogous to Fig.6a.

The above discussion shows that the characteristic features of ^{159}Yb decay scheme can be explained in quite some detail in terms of the non-interacting quasiparticle approach. This standard interpretation is also given by Courtney et al.[13]. Yet, there are also shape effects predicted by theory which go slightly beyond that scheme and which will be discussed in Sec.V for both ^{159}Yb and ^{160}Yb nuclei.

A synthetic representation of the alignment properties found in ^{159}Yb will also be given and compared with analogous results for ^{160}Yb in Sect.IV b, cf.Figs.8a-b.

IV. Results for ^{160}Yb

In this section some properties of the ^{160}Yb decay scheme and its interpretation will be discussed.

IVa. Experimental results for ^{160}Yb

The decay scheme for ^{160}Yb is relatively very well known from the work of Riedinger and his collaborators both at medium[11] and high[12] spins. The data we obtained in this experiment makes a contribution to only the yrast positive parity levels and to the two lowest negative parity bands. A decay scheme for ^{160}Yb is given in Fig.7a where the full complexity[12] of the decays out of the negative parity bands to the yrast states is not shown.

The positive parity yrast levels are observed to 40^+. No obvious irregularity in the band structure is observed in Fig.7a above the proton backbending. The 1158 keV decay of the 40^+ state is clearly seen in Fig.7b, the spectrum of γ-rays in coincidence with the 1078 decay of the 38^+ yrast state. Also the spectrum gated by the 1158 keV transition itself contains only γ-rays from the 38^+ and subsequent yrast levels.

For the odd-spin negative parity band our decay scheme agrees with previous work[13] up to the 31^- level but we find that the 878 keV γ-ray is not only a doublet with the decay of the yrast 32^+ level but it also has an extra

transition from the decay of the next level in this negative parity band. This may be seen from Fig.7c which shows that the 877-878 keV peak is self coincident. Detailed examination of the spectra in coincidence with known transitions in this band, and indeed the strength of the 878 keV peak in Fig. 7c, show that the 878 and 877 keV γ-rays occur sequentially from the 31^- and 33^- levels. Hence the 903 keV transition seen in previous work[13] is from the 35^- level.

The lowest negative parity band with even spin had previously been established up to spin 28^-. We do not observe a 744 keV decay[11] from the 20^- level but find that this transition has an energy of 781 keV, which is the same energy as one of the decays from the bottom of the band to the yrast states (8^- to 7^- to 6^+ giving 436 and 780 keV γ-rays) and also the 778 keV decay of the 26^- level higher in the band. Our data do not give an unambiguous order to the 688 and 712 keV γ-rays from the 22^- and 24^- levels, but we think the sequence shown in Fig.7a is the most probable.

IVb. Comments on the band structure in ^{160}Yb

The interpretation of the band structure in ^{160}Yb in terms of the quasiparticle assignments can be made using diagrams 6a-b, Sec.III.b, in full analogy to a similar interpretation for ^{159}Yb given there. Since detailed interpretation of this type was given in Refs.[11,12] and has also been discussed in a general context in Ref.[6], it will not be repeated here. Moreover, the low, and moderately high spin states in ^{160}Yb were a subject of main concern in the theoretical studies[17,18] where both the variation of pairing correlations[17] and deformation driving forces[18] have been analysed.

Therefore we limit ourselves here to a recapitulation of the nucleonic alignment properties, Fig.5,8a-b, which summarise the present experimental knowledge about characteristic frequencies and the aligned angular momentum values in both Ytterbium nuclei studied here.

V. Coherent valence particle alignment and its influence on the collective rotation.

In this discussion the particles outside the Z = 64 and N = 82 "core" are referred to as valence. There are therefore 6 valence protons and 7 and 8 valence neutrons in ^{159}Yb and ^{160}Yb, respectively. Despite the relatively large number of valence particles the alignment process is expected to enforce the shape change from prolate-collective to oblate-non-collective pattern as illustrated in Fig.1. This process, as we will argue, is accompanied by the band termination effect and possibly strengthened shape oscillations at certain spin values.

V.1. Shape change and band terminations.

There are at least two types of the prolate-to-oblate shape change mechanism predicted by theory. One, according to which the lowest energy sequence of given parity and signature undergoes a number of band crossings, every next band having γ-deformation closer to the $\gamma = 60°$ value.

A second mechanism according to which it is the original configuration whose shape smoothly evolves into a $\gamma = 60°$ shape without band crossings on the way. *The latter is referred to as a band termination mechanism.*

The cranking model analysis of the harmonic oscillator behaviour predicts[19,20] that any collectively rotating prolate deformed configuration built up of the harmonic oscillator states is going to evolve with increasing rotational frequency towards an oblate shape according to the above band-termination picture. The corresponding "final" oblate shape configuration is predicted to have a non-collective particle-hole structure. It corresponds, in terms of the spherical shell model, to a maximum alignment of the individual-j (single particle) angular momenta with the symmetry axis so that the symmetry axis and total angular momentum are nearly parallel.

The realistic average field potentials predict such a shape evolution mechanism as well, but only for a few nuclei along the periodic table. Most of the prolate-to-oblate shape changes are expected to be of the first kind mentioned above. In particular, the realistic calculations predict prolate-to-oblate shape transitions only in nuclei with a few valence nucleons in excess to spherical shell closures. In nuclei "from the middle of the shell" the competition with other shape transition modes (notably fission) is expected to be strong and offer better accomodation of the excitation energy.

We performed calculations of the expected shape evolution scheme using the Strutinsky method. The results of the calculation are summarised in Fig.9 for ^{159}Yb nucleus (technical details about the approach can be found in Ref.[21] and references therein). The results in Fig.9 correspond to a complete neglect of pairing but such a simplifying assumption is expected to be sufficient when the global features of the excitation at high and moderately high spins are studied. Comparison with experimental data (see inset in the Figure) shows that indeed the neglect of pairing offers a very good approximation there.

There are three characteristic global features to be seen from Fig.9. Firstly, in all possible parity-signature combinations ($\pi=\pm1,\alpha=\pm1/2$) there are two distinct shape configurations predicted. Collective ones, with $\beta_2 \sim 0.22$ and a small triaxility ($0 \lesssim \gamma \lesssim 5°$) give rise to the bands represented by the lines in the Figure. The noncollective ones, with $\beta_2 \sim 0.100$ to 0.260 and $\gamma = 60°$ give rise to an irregular excitation pattern and are represented by isolated symbols.

Secondly, at the high spin limit the oblate-shape non-collective coupling scheme is predicted to dominate at and near the yrast line. A characteristic envelope "moment of inertia" undergoes an evident structural change in the $I \sim 65/2$ to 71/2 spin range.

Thirdly, the collective bands are predicted to terminate at the following limiting spin values :

$$(\pi=+1,\alpha=+1/2) \quad I^{\pi} = 73/2^{+}$$

$$(\pi=+1,\alpha=-1/2) \quad I^{\pi} = 71/2^{+}$$

$$(\pi=-1,\alpha=+1/2) \quad I^{\pi} = 69/2^{-}$$

$$(\pi=-1,\alpha=-1/2) \quad I^{\pi} = 71/2^{-}.$$

(In the figure, the limiting points I^{π} are connected to the bands of the corresponding symmetry which demonstrates the effect in a dramatic way).

In order to gain an understanding of the microscopic structural features leading to a global scheme represented in Fig.9 it is instructive to study the maximum alignment configurations (sometimes referred to as "optimal"). In order to calculate the structure of the maximum alignment configurations we applied the tilted Fermi surface method of Ref.[3] in the realisation of Ref.[22] (for technical details and further references cf. Refs.[3,6,22]; here we only mention that the monopole pairing interaction was taken into account by employing the usual BCS procedure with blocking and that the approximate projection onto good particle number was performed). The results indicate that in particular the states $I^{\pi} = 69/2^{-}$, $71/2^{+}$, $71/2^{-}$ and $73/2^{+}$ candidate as band terminators. In all the bands displayed in Fig.9 the approach to the above maximum alignment configurations manifests itself in a similar way. The originally stable deformations (β,γ) begin to vary noticeably with spin: usually β_2 decreases to $\sim$ 0.15 and the instability in γ-deformation becomes pronounced. At the terminating spin configurations there are only non collective (maximum alignment) minima left with $\gamma = 60°$ and $\beta_2 \sim 0.15$. Corresponding results for ^{160}Yb are illustrated in Fig.10.

The predicted prolate-to-oblate shape transition and the accompanying band termination effects in nuclei with N ~ 90 originate from the rearrangements in the single-particle spectrum occuring for I ~ (30 to 50). Two kinds of rearrangements due to increasing rotation play a role in this context:

a. An increase or decrease in the single particle level density, in the vicinity of the actual Fermi level. Decrease in the level density (caused e.g. by an occurence of a significant gap in the single particle spectrum) causes, according to the Strutinsky approach, a stronger binding at the deformation and frequency range where it occurred. If the effect is strong enough a local minimum in the potential energy surface is created thus possibly giving rise to a shape-isomeric configuration.

b. The appearance or disappearance in the vicinity of actual Fermi level of highly alignable orbitals (those with large j and extreme m_j, i.e. small m_j for collective prolate-type configurations and big m_j for a non-collective $\gamma \approx 60°$ oblate shape configurations). Presence of such states, very favoured in energy, causes configuration changes with a strong increase in the aligned angular momentum. When two or more shape configurations compete, the number of occupied high-j orbitals often decides which of the configurations becomes lowest in energy.

By analysing the relevant single-particle spectrum diagrams one can understand first what is the microscopic origin for a predicted shape transition and which kind of nucleons (neutrons or protons) bring a stronger initiative in the single-particle rearrangement. The results of such calculations are presented in Figs. 11a-b and 12a-b.

Figure 11a represents the neutron single particle Routhians at a typical deformation corresponding to a collective band with $\gamma \approx 0°$ rotation in the

discussed ytterbium nuclei. A significant lowering of the level density occurs at N = 89,90,91 above the relatively high density area originating from K^{π} = $1/2^-$, $11/2^-$ and $3/2^-$ orbitals. In Fig.11b the analogous plot appropriate for non-collective $\gamma=60°$ configurations is given: at a complementary frequency range the N = 91 gap opens up and the low-density area soon includes also N = 89,90 gaps.

Following this way of reasoning we can then read from Fig.12a, analogous to Fig.11a, that a noticeable proton gap at Z = 70 extending from $\hbar\omega \approx 0$ terminates at $\hbar\omega \sim 0.45$. No particularly strong shell structure is predicted at Z = 70 at the oblate $\gamma = 60°$ shapes, as illustrated in Fig. 12b, but some lowering of the level density there is also clearly visible at high rotational frequency.

Summarising this part of the discussion: there are coherent prolate shape stabilising shell effects due to both neutrons and protons which for discussed particle numbers terminate, as a function of rotational frequency at $\hbar\omega \sim 0.45$ MeV in both types of nucleons. In addition, there are relatively strong shell effects at the oblate shape configuration for $\hbar\omega > 0.45$ MeV which imply the prolate-to-oblate shape transition (compare with the general band structure in Figs.9,10).

A characteristic lowering of the oblate shape configuration energies at I > 71/2 (I > 35), cf. Fig.9 (Fig.10), is due to the fact that in the corresponding wave functions there are already three highly "alignable" orbitals, viz. $i_{13/2,K=13/2}$, $i_{13/2,K=11/2}$ and $i_{13/2,K=9/2}$ below the Fermi level; cf. Fig.11b. The oblate shape configurations, at I < 71/2 (I>30) in Fig.9 (Fig.10) do not in general contain an $i_{13/2,K=9/2}$ orbital. Similarly, the configurations of the collectively rotating states have from the beginning up

to the termination point two $i_{13/2}$ orbitals occupied. These at $\gamma = 0°$ bring nearly identical alignment as the $i_{13/2,K=13/2}$ and $i_{13/2,K=11/2}$ orbitals at $\gamma = 60°$.

V.2. The effect of the valence particles on a collective rotation

The experimental results for the nuclei studied here reveal characteristic deviations from the $I(I+1)$ rule above the frequency $\hbar\omega \approx (0.40$ to $0.43)$ MeV at which the first proton alignment takes place.

In order to analyse the physical nature of these deviations we performed a systematic calculation of the theoretical energy spectra assuming for a moment that the nuclei in question are already oblate. (The method used is the same as the one quoted in Sec.VI when discussing the maximum alignment configurations and band terminators).

It is known[23] that such an oblate shape level sequence often reveals characteristic fluctations when plotted in E-vs.-I representation, states with the so-called optimal configurations lying particularly low in energy. We performed these calculations for ^{159,160}Yb.

The results of the calculation are compared to the experimental data on ^{159}Yb in Fig.13. Since the systematic deviations from the $I(I+1)$ rule are of the order of a few dozens of keV in this case, we magnify the effect of variation of E in function of I by plotting the derivative dE/dI instead. A comparison has been done for the $\alpha=+1/2$ $\pi=+1$ and $\pi=-1$ bands in ^{159}Yb. (A similar correlation although slightly weaker, is also present for the $\pi=-1$, $\alpha=-1/2$ band). Here the resemblance of the two patterns is again very clear,

especially the "oscillation-type" pattern around $I^{\pi} = 49/2^{+}$ and $I^{\pi} = 57/2^{-}$, for $\pi=+1$ and $\alpha=+1/2$, and $\pi=-1$ $\alpha=+1/2$ bands, respectively. (Obviously the backbending manifests itself in such a representation as a lowering the lines as well). The characteristic states have the following properties:

$$I^{\pi} = 49/2^{+} : \nu(i^{3}_{13/2})^{max}_{33/2} \otimes h^{max}_{9/2} \otimes f^{max}_{7/2} ;$$

$$I^{\pi} = 57/2^{-} : \nu(i^{2}_{13/2})^{max}_{12} \otimes h^{max}_{9/2} \otimes \pi(h^{6}_{11/2})^{max}_{12..}.$$

Here and in the following we simplify the notation by indicating only those particles which contribute a non-zero angular momentum to the total spin. The pairs of particles coupled to zero play a particular role in our formalism which employs the monopole-pairing force. Such pairs may cause an additional binding due to the attractive pairing force and lower the energy of the corresponding configuration. We indicate their presence in partly occupied orbitals with the double-dot symbol$^{\cdot\cdot}$. For instance we write $(h^{6}_{11/2})^{max}_{12..}$ to indicate, that two orbitals, viz. those with K = + 11/2 and K = - 11/2 are coupled to zero within their $h_{11/2}$ subshell, while the remaining four particles exhaust the alignment up to its maximum permitted by the Pauli principle.

Similar correlations between the maximum alignment configurations at $\gamma = 60°$ and lowering of levels in the collective bands although as expected weaker, take place for ^{160}Yb, cf. Fig.14, where the anologous comparison for the yrast band is made. Here a characteristic fluctuation takes place around $I^{\pi} = 36^{+}$. The optimal $I^{\pi} = 36^{+}$ state has the structure :

$$I^{\pi} = 36^{+} : \nu(i^{2}_{13/2})^{max}_{12} \otimes (h^{3}_{9/2})^{max}_{21/2} \otimes (f^{3}_{7/2})^{max}_{15/2} \otimes \pi(h^{6}_{11/2})^{max}_{6..},$$

while another one, also optimal,

$$I^{\pi} = 36^{+}_{2} : \nu(i^{2}_{13/2})^{max}_{12} \otimes (h^{2}_{9/2})^{max}_{8} \otimes (f^{4}_{7/2})^{max}_{4} .. \otimes \pi(h^{6}_{11/2})^{max}_{12} ..$$

is calculated to lie slightly higher in energy, see also ref.[14].

The abundance of maximum alignment configurations strongly increases with increasing spin. This is because of the relatively large number of valence nucleons available. Below we present a few examples. For instance we find the states :

$$I^{\pi} = 38^{+} : \nu(i^{2}_{13/2})^{max}_{12} \otimes (h^{2}_{9/2})^{max}_{8} \otimes (f^{2}_{7/2})^{max}_{6} \otimes \pi(h^{6}_{11/2})^{max}_{12} ..$$

and

$$I^{\pi} = 38^{-} : \nu(i^{2}_{13/2})^{max}_{12} \otimes (h^{2}_{9/2})^{max}_{8} \otimes (f^{2}_{7/2})^{max}_{6} \otimes \pi(h^{5}_{11/2} d_{3/2})^{max}_{12} ..$$

with nearly degenerate energy values. Only above 100 keV higher another maximum alignment configuration is predicted :

$$I^{\pi} = 38^{-} : \nu(i^{3}_{13/2})^{max}_{33/2} \otimes (f^{3}_{7/2})^{max}_{15/2} \otimes (h^{2}_{9/2})^{max}_{8} \otimes \pi(h^{6}_{11/2})^{max}_{6} ::$$

In the above configuration there is only one proton-pair broken and some proton pairing contribution lowering its energy is likely.

For I = 40 we find also :

$$I^{\pi} = 40^{+} : \nu(i^{3}_{13/2})^{max}_{33/2} \otimes (f_{7/2})^{max}_{7/2} \otimes (h^{2}_{9/2})^{max}_{8} \otimes \pi(h^{5}_{11/2} d_{3/2})^{max}_{12} ..$$

and

$$I^{\pi} = 40^{-} : \nu(i^{3}_{13/2})^{max}_{33/2} \otimes (f_{7/2})^{max}_{7/2} \otimes (h^{2}_{9/2})^{max}_{8} \otimes \pi(h^{6}_{11/2})^{max}_{12} ..$$

and further on

$$I^{\pi} = 42^{-} : \nu(i^{2}_{13/2})^{max}_{12} \otimes (h^{3}_{9/2})^{max}_{21/2} \otimes (f^{3}_{7/2})_{15/2} \otimes \pi(h^{5}_{11/2}, d_{3/2})^{max}_{12}..$$

$$I^{\pi} = 42^{+} : \text{where } \pi(h^{5}_{11/2}, d_{3/2})^{max}_{12}.. \text{ is replaced by } \pi(h^{6}_{11/2})^{max}_{12}..$$

To compare the maximum alignment configuration pattern with the experimental data available an illustration analogous to that in Fig.13 is given, cf. Fig.15. Here we use the experimental results on the negative parity side bands in ^{160}Yb; since the discussed fluctuations are of a very small amplitude in this case, we represent the quantity d^2E/dI^2 calculated from the experimental level energies using the usual finite difference approximation. A lowering of the corresponding curve at $I^{\pi} = 38^{-}$ and 40^{-} may be viewed as the effect of coherent alignment in orbitals indicated above although the theoretical $I^{\pi} = 40^{-}$ point lies slightly too high. The characteristic fluctuations are also present in $\pi = -1$ $\alpha = 1$ band (cf. top part of Fig.15) but the higher lying (yet unobserved) transitions would be useful to complete the systematics.

The results presented here (cf. Figs. 13-15) indicate not only the lowering of energies of the collectively rotating states at the maximum alignment configurations but also a correlation with the other states of the $\gamma = 60°$ symmetry. In qualitative terms : if the states are calculated (at $\gamma = 60°$) to lie higher (lower) in energy, the states of the corresponding spins are measured to lie higher (lower) in energy as well.

Theoretical calculations explain the decrease in the intensity of the effect discussed when the neutron number increases from N = 88 to N = 90 by increasing prolate-oblate energy difference and increasing difference between the numbers of occupied high-j orbitals at prolate and oblate shape. For heavier isotopes the energy of the oblate shape configuration with respect to

that of the collective one increases quickly reaching $\Delta E \sim 4$ MeV at ^{168}Yb, (Fig.1). The numbers of occupied $i_{13/2}$ neutron orbitals for ^{160}Yb at high frequencies are 6 and 4 at prolate and oblate shapes respectively, see Fig.11. Therefore no effect of correlation is present in ^{168}Yb, and other "γ-stiff" rotor nuclei. The ^{168}Yb results reveal no deviation from I(I + 1) rule (in the energy scale discussed here).

VI. Summary and Conclusions.

The most spectacular feature of the experimentally observed spectra is the tendency to systematically deviate from the I(I+1) rule above the proton backbending frequency. As has been noticed in other $N \sim 90$ nuclei[14] these deviations are the strongest for those spins which correspond to the maximum alignment of angular momentum possible at a given particle (hole) configuration. A mechanism which could explain this interesting new feature involves most likely a simultaneous effects from alignment and shape coexistence at high spins.

The possible oblate and prolate shape coexistence gives most likely rise to the interaction between the corresponding quantum mechanical states. The energies of the maximum alignment configurations (sometimes referred to as the "yrast trap" configurations) are known to be particularly low; the corresponding interaction is likely to push the collective yrast levels lower, thus explaining[14] the observed deviations. The magnitude of interaction between prolate and oblate structures obviously depends on a similarity between corresponding wave functions. Theoretical calculation of such interaction goes, however, beyond the framework of this article.

In both of the two nuclei we have studied here we are seemingly witnessing a coherent influence of the bulk of the valence particles (a maximum of 13 to 14 in the nuclei studied). With the tendency of the valence particles to align the maximum angular momentum allowed by the Pauli principle, the γ-soft core does not seem to rigidly resist a polarisation which manifests itself in a systematic way as deviations from the I(I+1) pattern.

Acknowledgments

W.N. gratefully acknowledges support from the Danish Research Council during his stay at the NBI. This work was supported by the UK Science and Engineering Research Council (SERC). HWC-G and DH acknowledge the receipt of SGRC postgraduate studentships. MAR acknowledges support from the Royal Society.

References

1) A.Bohr and B.R.Mottelson, Phys.Scr.10A (1974) 13

2) R.Bengtsson, S.E.Larsson, G.Leander, P.Møller, S.G.Nilsson, S.Åberg and Z.Szymanski, Phys.Lett.57B (1975) 301

3) G.Andersson, S.E.Larsson, G.Leander, P.Møller, S.G.Nilsson, I.Ragnarsson, S.Åberg, R.Bengtsson, J.Dudek, B.Nerlo-Pomorska, K.Pomorski, and Z. Szymanski, Nucl.Phys.A268 (1976) 205

4) G.Andersson, R.Bengtsson, T.Bengtsson, J.Krumlinde, G.Leander, K. Neergaard, P.Olanders, J.A.Pinston, I.Ragnarsson, Z.Szymanski and S. Åberg, Phys.Scr. 24 (1981) 266
T.Bengtsson and I.Ragnarsson, Nucl.Phys.A436 (1985)14

5) J.Dudek and W.Nazarewicz, Phys.Rev.C31 (1985) 982

6. M.de Voigt, J.Dudek and Z.Szymanski, Rev.Mod.Phys.55 (1983) 949

7. C.Baktash, Y.Schutz, I.Y.Lee, F.K.McGovan, N.R.Johnson, M.L.Halbert, D.C.Hensley, M.P.Fewell, L.Courtney, A.J.Larabee, L.L.Riedinger, A.W.Sunyar, E.der Mateosian, O.C.Kistner and D.G.Sarantites, Phys. Rev.Lett. 54 (1985) 978;
S.B.Patel, F.S.Stephens, J.C.Bacelar, E.M.Beck, M.A.Deleplanque, R.M. Diamond and J.E.Draper, Phys.Rev.Lett.57 (1986)62

8. I.Ragnarsson, T.Bengtsson, W.Nazarewicz, J.Dudek and G.A.Leander, Phys.Rev.Lett. 54 (1985) 982

9. J.Simpson, M.A.Riley, J.R.Cresswell, F.D.Forsyth, D.Howe, B.M.Nyako and J.F.Sharpey-Schafer, J.C.Bacelar, J.D.Garrett, G.B.Hagemann, B.Herskind and A.Holm, Phys.Rev.Lett. 53 (1984) 648;
see also further experimental confirmation in:
P.O.Tjøm, R.M.Diamond, J.C.Bacelar, E.M.Beck, M.A.Deleplanque, J.E.Draper, and F.S.Stephens, Phys.Rev.Lett. 22 (1985) 2405

10. F.A.Beck, E.Bozek, T.Byrski, C.Gehringer, J.C.Merdinger, Y.Schutz, J.Styczen and J.P.Vivien, Phys.Rev.Lett.42 (1979) 493

11. L.L.Riedinger, O.Andersen, S.Frauendorf, J.D.Garrett, J.J.Gaardhøje, G.B.Hagemann, B.Herskind, B.Makovetzky, J.C.Waddington, M.Guttormsen and P.O.Tjørm, Phys.Rev.Lett.44 (1980) 568

12. L.L.Riedinger, Nucl.Phys.A347 (1980) 141 and Phys.Scr.24 (1981) 312

13. L.H.Courtney et al., Progress Report on Nuclear Spectroscopic Studies, The University of Tennessee, June 1984-May 1985, p.8 and June 1985-May 1986, p.46

14. M.A.Riley, J.D.Garrett, J.F.Sharpey-Schafer and J.Simpson, Phys.Lett.B177 (1986)15.

15. P.J.Twin, P.J.Nolan, R.Aryaeinejad, D.J.G.Love, A.H.Nelson and A.Kirwan, Nucl.Phys.A409 (1983) 343c

16. T.Byrski, F.A.Beck, C.Gehringer, J.C.Merdinger, Y.Schutz, J.P.Vivien, J.Dudek, W.Nazarewicz and Z.Szymanski Phys.Lett.102B (1981) 235

17. S.Cwiok, W.Nazarewicz, J.Dudek, J.Skalski, and Z.Szymanski ; Nucl.Phys.A333 (1980) 139

18. R.Bengtsson, S.Chen, J.-Y.Zhang and S.Åberg, Nucl.Phys.A405 (1983) 221

19. A.Bohr and B.R.Mottelson, Nuclear Structure, Vol.II, W.A.Benjamin Inc., 1975

20. Z.Szymanski, Fast Nuclear Rotation, Clarendon Press, Oxford, 1983.

21. W.Nazarewicz, J.Dudek, R.Bengtsson, T.Bengtsson and I.Ragnarsson, Nucl.Phys.A435 (1985) 397

22. J.Dudek, Z.Szymanski, J.Werner, A.Faessler and C.Lima, Phys.Rev.C26 (1982) 1712

23. J.Dudek, Proc.Int.Conf. in Nuclear Physics, Strasbourg 1980, J.Phys. (Paris) Colloq.41-10, 18

Figure Captions.

Fig.1 Predicted total energy behaviour in the (β,γ)-plane at $I^{\pi}=30^{+}$ for $_{70}Yb_{88-98}$ nuclei. While the heavier ($N \geq 92$) isotopes possess well defined minima on the $\gamma \approx 0°$ axis, ^{160}Yb reveals a prolate/oblate shape coexistence at this spin. The nucleus ^{158}Yb is predicted to be "γ-soft" with the preference for oblate shape equilibrium. (The coordinate system used is the following: vertical-upwards (downwards) oriented axis corresponds to $\gamma = 60°$ ($\gamma=-120°$) noncollective axially-symmetric and oblate (prolate) shape rotation. The two intermediate axes correspond to $\gamma=0°$ and $\gamma=-60°$ axially-symmetric prolate-shape collective and oblate-shape collective configurations.

Fig.2 Total energy (ΣE_{γ}) detected by the BGO crystal ball vs. fold: a. 5n channel (^{159}Yb) ; b. 4n channel (^{160}Yb).

Fig.3 The decay scheme of ^{159}Yb as found in this work.

Fig.4a This and the following figures 4b-e show examples of coincidence spectra used to construct the decay scheme of Fig.3. Here, spectrum of γ-rays in coincidence with the 748, 790 and 774 keV transitions in the positive parity band is shown.

Fig.4b Spectrum of γ-rays in coincidence with the 774 keV ($45/2^{+}\rightarrow 41/2^{+}$) transition.

Fig.4c Spectrum of γ-rays in coincidence with the 481 keV ($29/2^{-}\rightarrow 25/2^{-}$) transition.

Fig.4d Spectrum of γ-rays in coincidence with the 714 keV ($45/2^{-}\rightarrow 41/2^{-}$) transition.

Fig.4e Spectrum of γ-rays in coincidence with the 811 keV ($59/2^{-}\rightarrow 55/2^{-}$) transition.

Fig.5 Measured W(30°)/W(90°) intensity ratios as a function of the γ-ray energy. The average value for previously known stretched E2 transitions is indicated by a dashed line.

Fig.6a The neutron quasiparticle spectrum (left-upper panel) and the pairing energy gap (left-lower panel) as a function of rotational frequency ω obtained using the approach of Ref.17.

Fig.6b Similar to Fig.6a but for the protons.

Fig.7a Partial decay scheme for ^{160}Yb.

Fig.7b Spectrum of γ-rays, in coincidence with the 1078 keV ($38^+ \rightarrow 36^+$) transition.

Fig.7c Spectrum of γ-rays in coincidence with the 878 keV multiplet ($32^+ \rightarrow 30^+$, $31^- \rightarrow 29^-$ and $33^- \rightarrow 31^-$) demonstrating its self coincident character.

Fig.8a Angular momentum alignment plot for the rotational bands in ^{159}Yb. The characteristic quasiparticle structures are indicated using the usual notation.

Fig.8b Similar to Fig.8a but for ^{160}Yb.

Fig.9 The calculated excitation pattern for ^{159}Yb represented in a form of energy vs. spin plot. For better fit in the plot area the energies are represented as relative to a parabola axI^2 with a = 0.006. The flag symbols indicate the spin values at which bands end. Lines connect the points of collective rotation and terminate at the first non-collective γ = 60° point. Circles and squares represent non-collective energies for the corresponding parity-signature combinations as represented in the legend. For comparison the experimental data are also shown (inset)continuous, dasjed and dotted lines according to the notation in the legend using the same reference constant a = 0.006. Pairing is neglected in the calculations. Similarity between the experimental and the

theoretical structure deserves noting : relative closeness of the negative parity bands and the crossing at I∿ 43/2ℏ with the positive parity yrast band.

Fig.10 Similar to Fig.9 but for ^{160}Yb.

Fig.11a Neutron single particle Routhians in function of rotational frequency at the deformation characteristic for the equilibrium shapes of ^{159}Yb and ^{160}Yb at low and moderately high spins. A low level-density area corresponding to particle numbers N∿ 89-91 terminates at ℏω ∿ 0.45 MeV to 0.60 MeV.

Fig.11b Complementary to that of Fig.11a, showing the opening of the lower level-density area at ℏω∿0.40 MeV onwards, for the neutron numbers N∿ 88 to 91, relevant for the present study. Note, per contrast, a typically high level-density area extending over the upper part of the diagram.

Fig.12a Similar to that in Fig.11a but for the protons.

Fig.12b Similar to that in Fig.11b but for the protons.

Fig.13 The theoretical energy vs. spin, for ^{159}Yb left-hand side scale, full circles, calculated at the $\gamma = 60°$ oblate shapes compared to the experiment, right-hand side scale, inverted triangles. The experimental data are represented in the form of the derivates $\omega \equiv dE/dI$ approximated as usually by the finite differences.

Fig.14 Similar to the results in Fig.13 but for the yrast line in ^{160}Yb. Here we use the $\pi=+1$, $\alpha=0$ band only.

Fig.15 Theoretical energy vs. spin dependence, left-hand side scale compared to the experimental results right-hand side scale, for lateral bands in ^{160}Yb.Here the effect in the experimental results is so much weaker that we decided to magnify the effect even more by plotting the second derivatives, d^2E/dI^2, right-hand scale. Experimental data represented by the inverted triangles.

SHAPE EVOLUTION

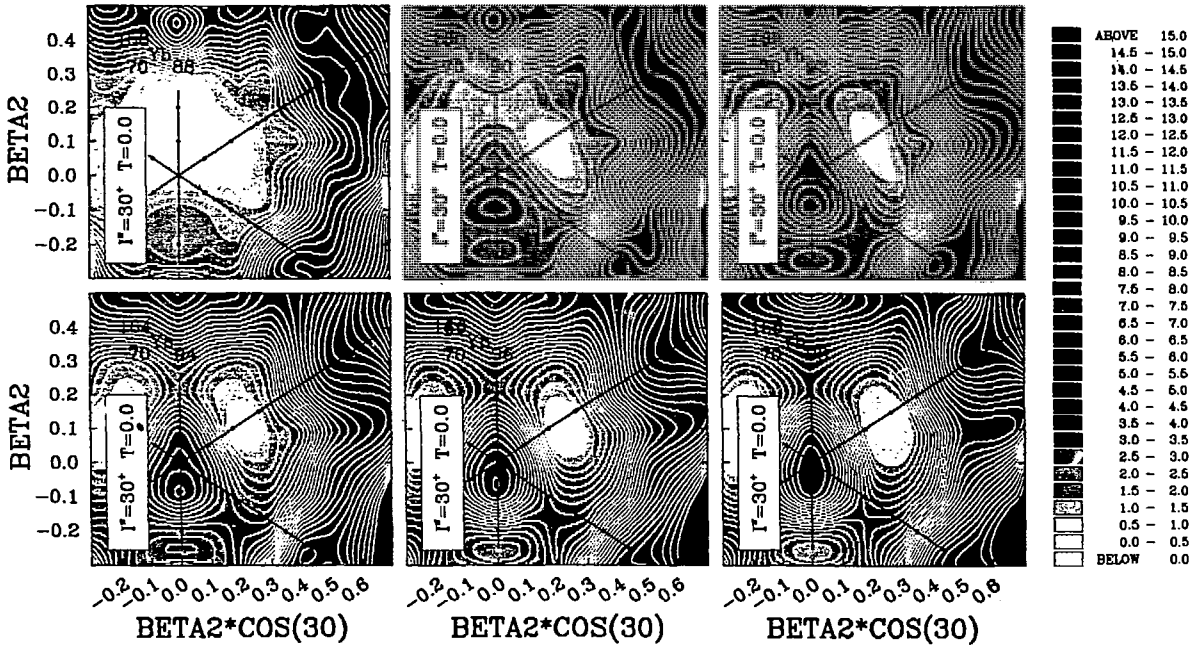

Fig. 1

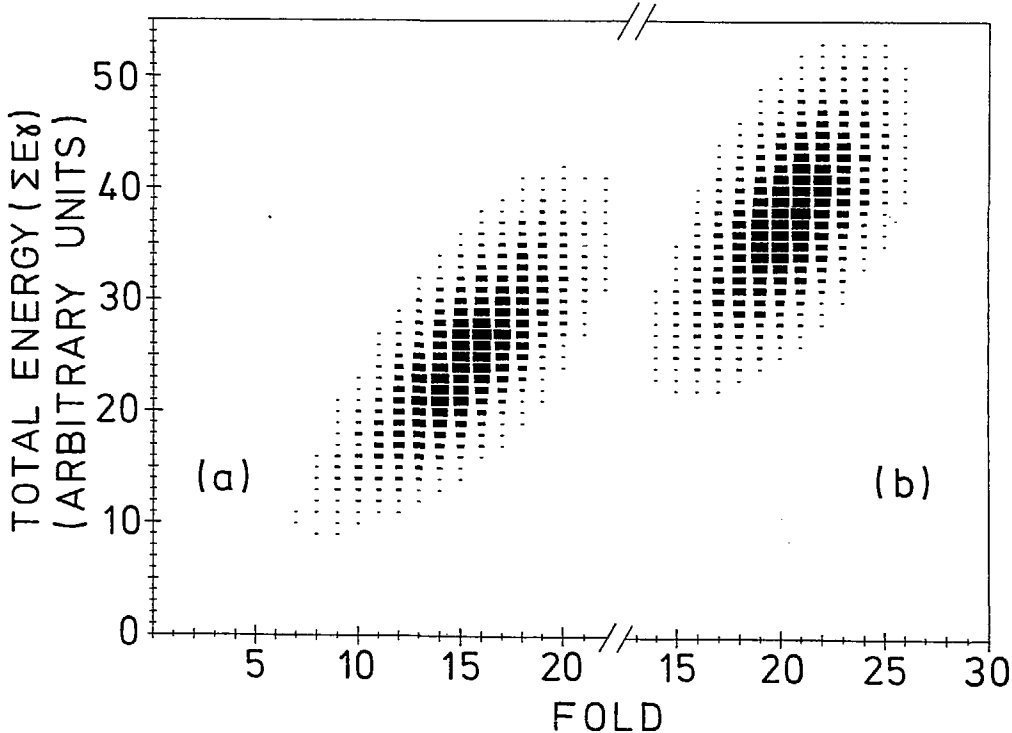
TOTAL ENERGY (ΣEγ)
(ARBITRARY UNITS)
50
40
30
20
10
0
(a)
(b)
5
10
15
20
15
20
25
30
FOLD

Fig.2

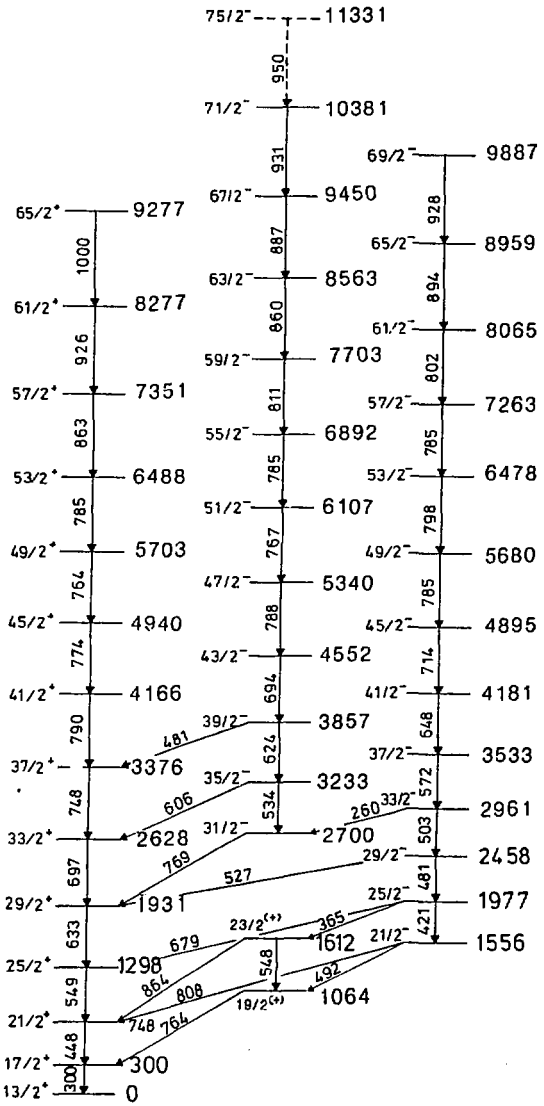
75/2⁻ 11331
950
71/2⁻ 10381
931
67/2⁻ 9450
887
63/2⁻ 8563
860
59/2⁻ 7703
811
55/2⁻ 6892
785
51/2⁻ 6107
767
47/2⁻ 5340
788
43/2⁻ 4552
694
39/2⁻ 3857
624
35/2⁻ 3233
534
31/2⁻ 2700
769
606
481
527
260
65/2⁺ 9277
1000
61/2⁺ 8277
926
57/2⁺ 7351
863
53/2⁺ 6488
785
49/2⁺ 5703
764
45/2⁺ 4940
774
41/2⁺ 4166
790
37/2⁺ 3376
748
33/2⁺ 2628
697
29/2⁺ 1931
633
25/2⁺ 1298
549
21/2⁺ 748
448
17/2⁺ 300
300
13/2⁺ 0
69/2⁻ 9887
928
65/2⁻ 8959
894
61/2⁻ 8065
802
57/2⁻ 7263
785
53/2⁻ 6478
798
49/2⁻ 5680
785
45/2⁻ 4895
714
41/2⁻ 4181
648
37/2⁻ 3533
572
33/2⁻ 2961
503
29/2⁻ 2458
481
25/2⁻ 1977
421
21/2⁻ 1556
679
864
808
764
365
548
492
23/2(+) 1612
19/2(+) 1064
159 Yb

Fig. 3

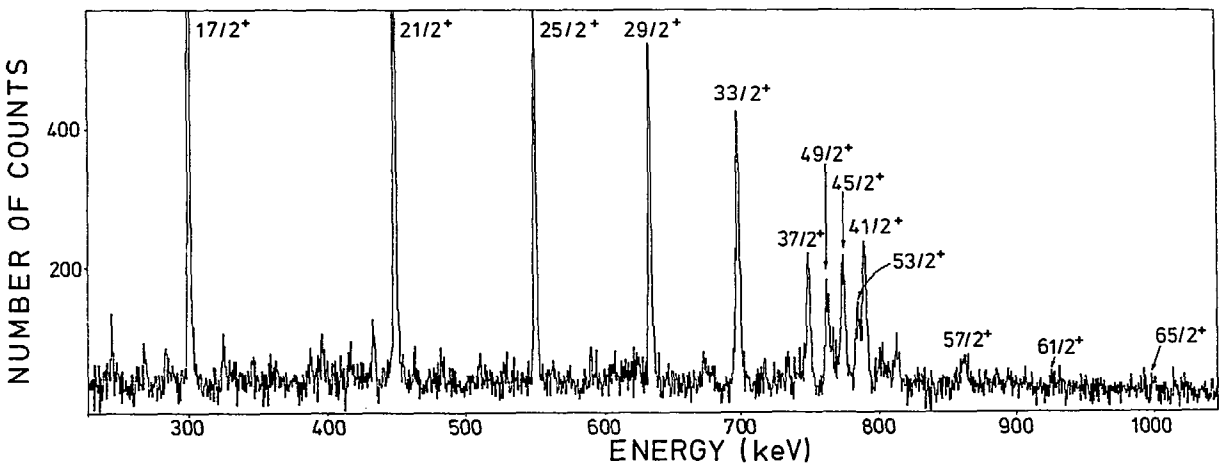
NUMBER OF COUNTS
400
200
17/2+
21/2+
25/2+
29/2+
33/2+
49/2+
45/2+
41/2+
37/2+
53/2+
57/2+
61/2+
65/2+
300
400
500
600
700
800
900
1000
ENERGY (keV)

Fig. 4 a

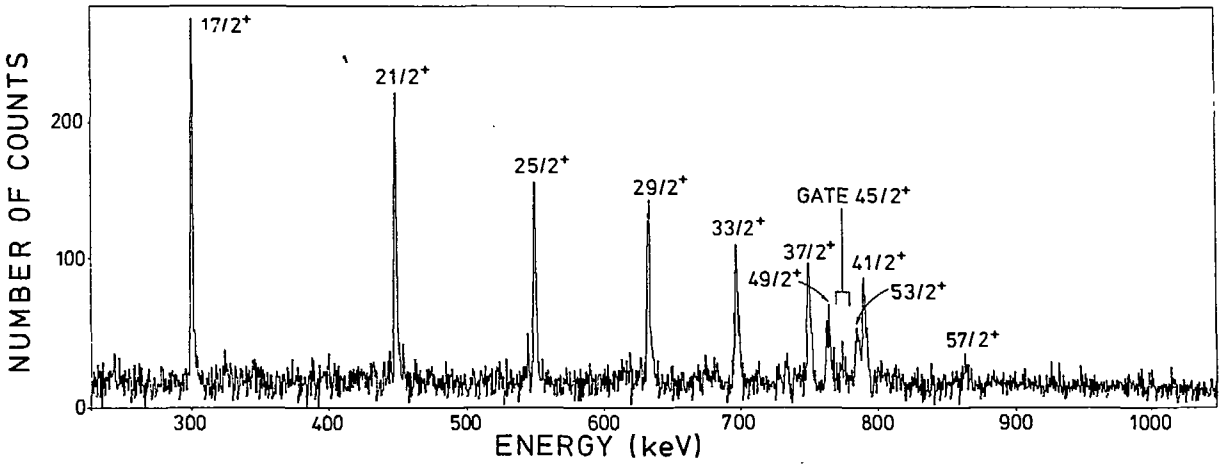
NUMBER OF COUNTS
0
100
200
300
400
500
600
700
800
900
1000
ENERGY (keV)
17/2+
21/2+
25/2+
29/2+
33/2+
GATE 45/2+
37/2+
41/2+
49/2+
53/2+
57/2+

Fig. 4 b

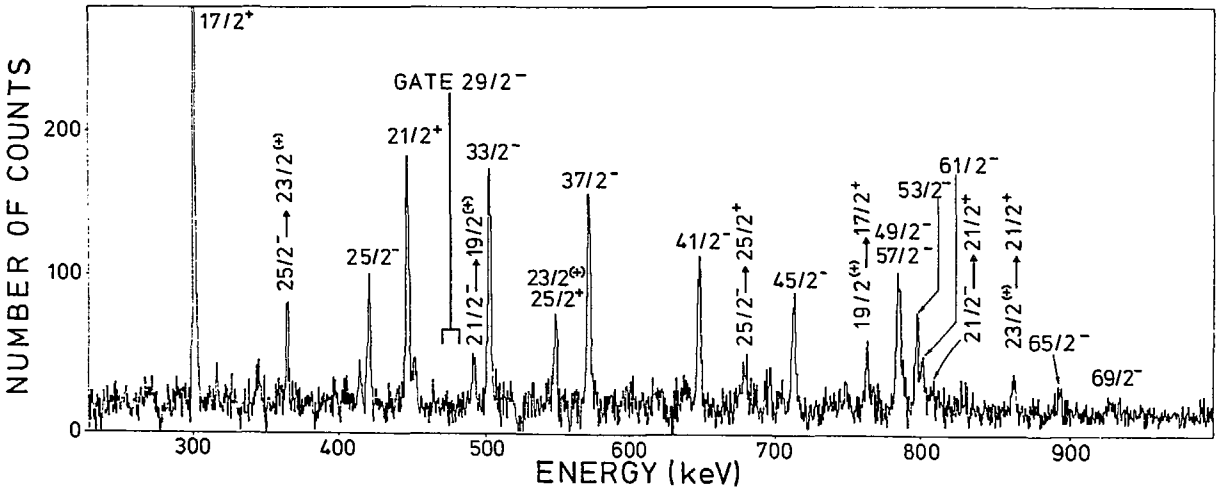
NUMBER OF COUNTS
0
100
200
300
400
500
600
700
800
900
ENERGY (keV)
17/2+
GATE 29/2−
21/2+
33/2−
37/2−
25/2−
41/2−
45/2−
61/2−
53/2−
49/2−
57/2−
65/2−
69/2−
25/2− → 23/2(+)
21/2− → 19/2(+)
23/2(+) 25/2+
25/2− → 25/2+
19/2(+) → 17/2+
21/2− → 21/2+
23/2(+) → 21/2+

Fig. 4 c

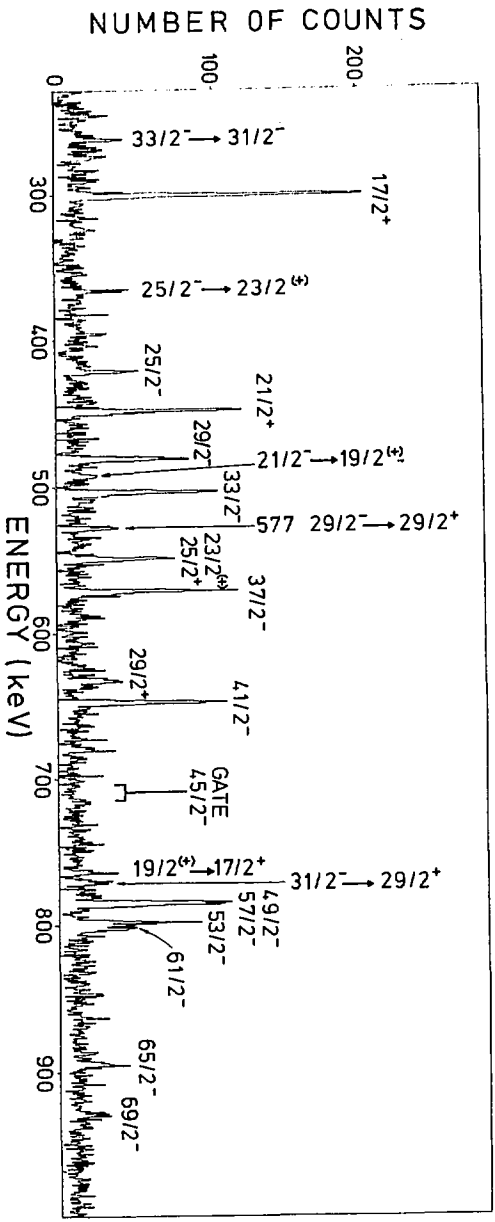
NUMBER OF COUNTS
0
100
200
ENERGY (keV)
300
400
500
600
700
800
900
33/2⁻ → 31/2⁻
17/2⁺
25/2⁻ → 23/2(+)
25/2⁻
21/2⁺
29/2⁻
21/2⁻ → 19/2(+)
33/2⁻
577 29/2⁻ → 29/2⁺
23/2(+)
25/2⁺
37/2⁻
29/2⁺
41/2⁻
GATE
45/2⁻
19/2(+) → 17/2⁺
31/2⁻ → 29/2⁺
49/2⁻
57/2⁻
53/2⁻
61/2⁻
65/2⁻
69/2⁻

Fig. 4 d

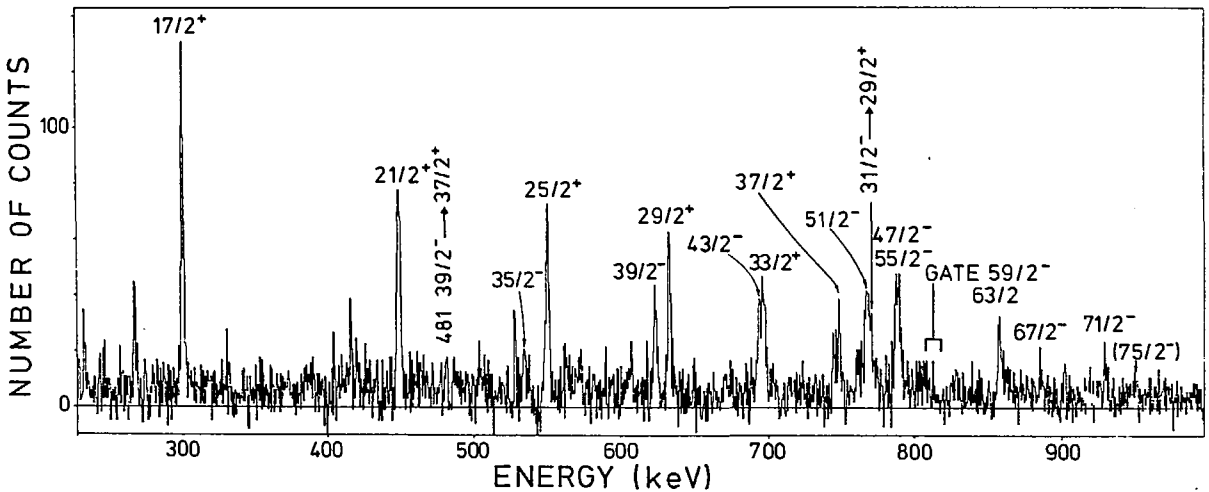
NUMBER OF COUNTS
100
0
17/2+
21/2+
481
39/2−→37/2+
25/2+
35/2−
39/2−
29/2+
43/2−
33/2+
37/2+
51/2−
31/2−→29/2+
47/2−
55/2−
GATE 59/2−
63/2
67/2−
71/2−
(75/2−)
300
400
500
600
700
800
900
ENERGY (keV)

Fig. 4 e

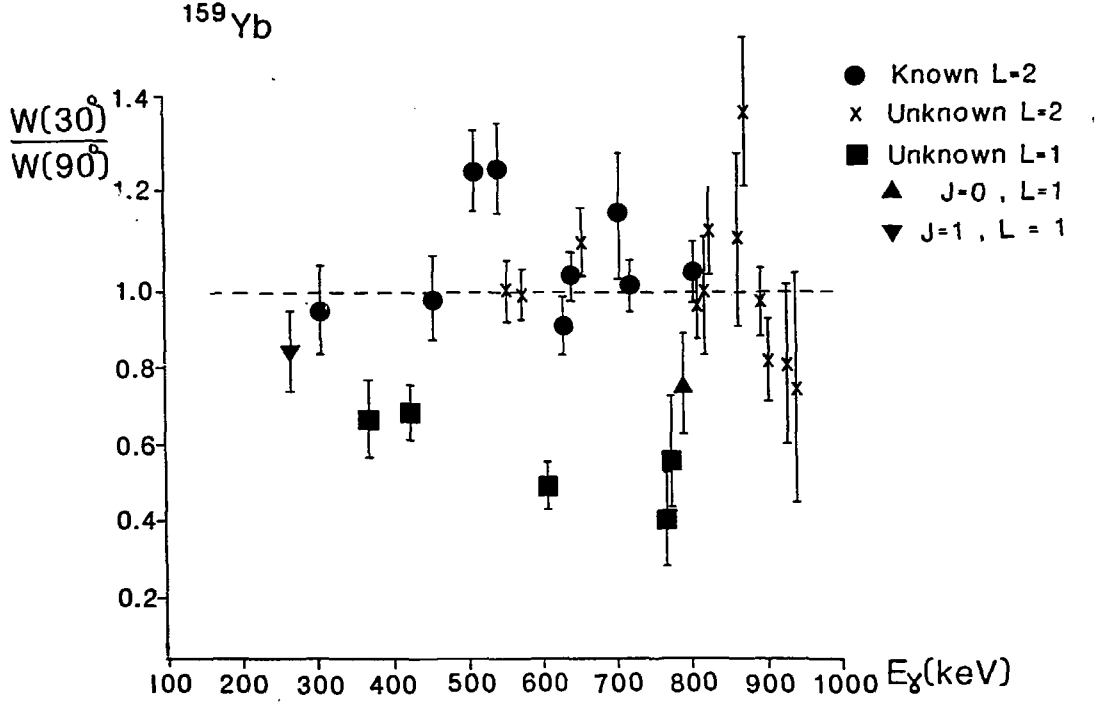
159Yb
W(30°)/W(90°)
1.4
1.2
1.0
0.8
0.6
0.4
0.2
100 200 300 400 500 600 700 800 900 1000
Eγ(keV)
Known L=2
Unknown L=2
Unknown L=1
J=0 , L=1
J=1 , L = 1

Fig. 5

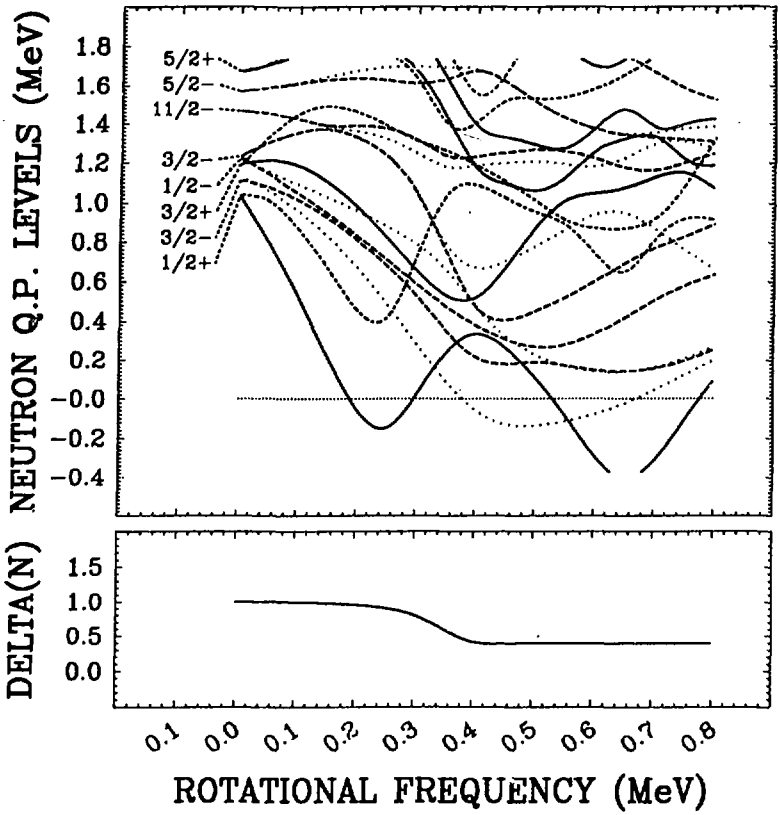
NEUTRON Q.P. LEVELS (MeV)
1.8
1.6
1.4
1.2
1.0
0.8
0.6
0.4
0.2
−0.0
−0.2
−0.4
5/2+
5/2−
11/2−
3/2−
1/2−
3/2+
3/2−
1/2+
DELTA(N)
1.5
1.0
0.5
0.0
0.1
0.0
0.1
0.2
0.3
0.4
0.5
0.6
0.7
0.8
ROTATIONAL FREQUENCY (MeV)

Fig. 6 a

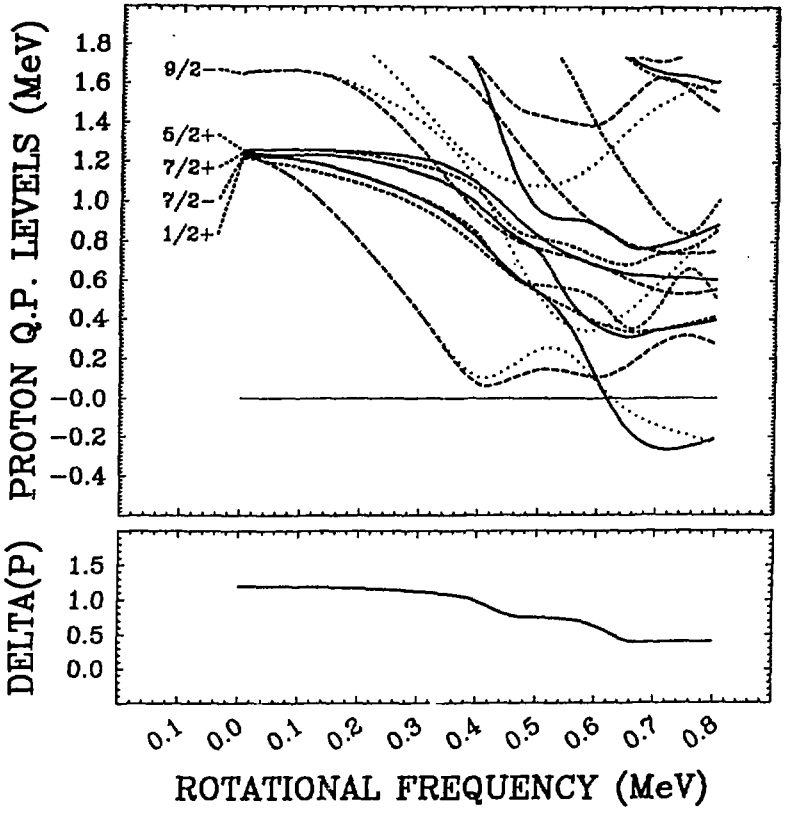
PROTON Q.P. LEVELS (MeV)
1.8
1.6
1.4
1.2
1.0
0.8
0.6
0.4
0.2
−0.0
−0.2
−0.4
9/2−
5/2+
7/2+
7/2−
1/2+
DELTA(P)
1.5
1.0
0.5
0.0
0.1
0.0
0.1
0.2
0.3
0.4
0.5
0.6
0.7
0.8
ROTATIONAL FREQUENCY (MeV)

Fig. 6 b

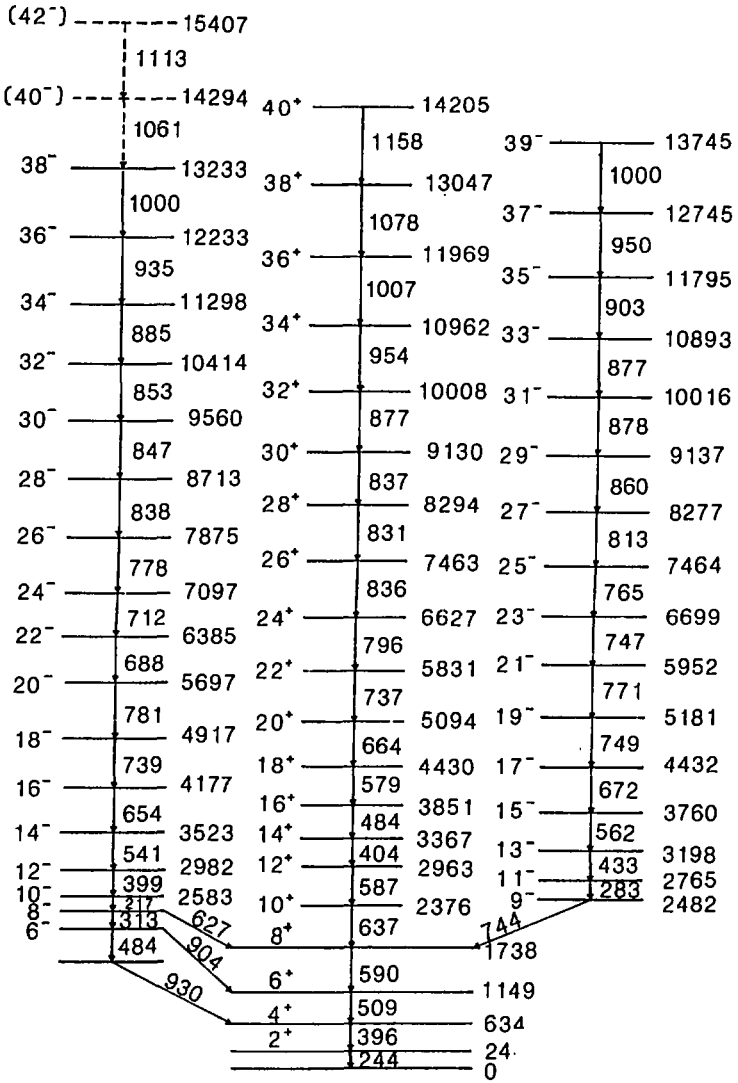
(42⁻) 15407
1113
(40⁻) 14294
1061
38⁻ 13233
1000
36⁻ 12233
935
34⁻ 11298
885
32⁻ 10414
853
30⁻ 9560
847
28⁻ 8713
838
26⁻ 7875
778
24⁻ 7097
712
22⁻ 6385
688
20⁻ 5697
781
18⁻ 4917
739
16⁻ 4177
654
14⁻ 3523
541
12⁻ 2982
399
10⁻ 2583
217
8⁻
313
6⁻
484
627
904
930
40⁺ 14205
1158
38⁺ 13047
1078
36⁺ 11969
1007
34⁺ 10962
954
32⁺ 10008
877
30⁺ 9130
837
28⁺ 8294
831
26⁺ 7463
836
24⁺ 6627
796
22⁺ 5831
737
20⁺ 5094
664
18⁺ 4430
579
16⁺ 3851
484
14⁺ 3367
404
12⁺ 2963
587
10⁺ 2376
637
8⁺
744
1738
6⁺ 590 1149
4⁺ 509 634
2⁺ 396 24
244 0
39⁻ 13745
1000
37⁻ 12745
950
35⁻ 11795
903
33⁻ 10893
877
31⁻ 10016
878
29⁻ 9137
860
27⁻ 8277
813
25⁻ 7464
765
23⁻ 6699
747
21⁻ 5952
771
19⁻ 5181
749
17⁻ 4432
672
15⁻ 3760
562
13⁻ 3198
433
11⁻ 2765
283
9⁻ 2482
160Yb

Fig. 7 a

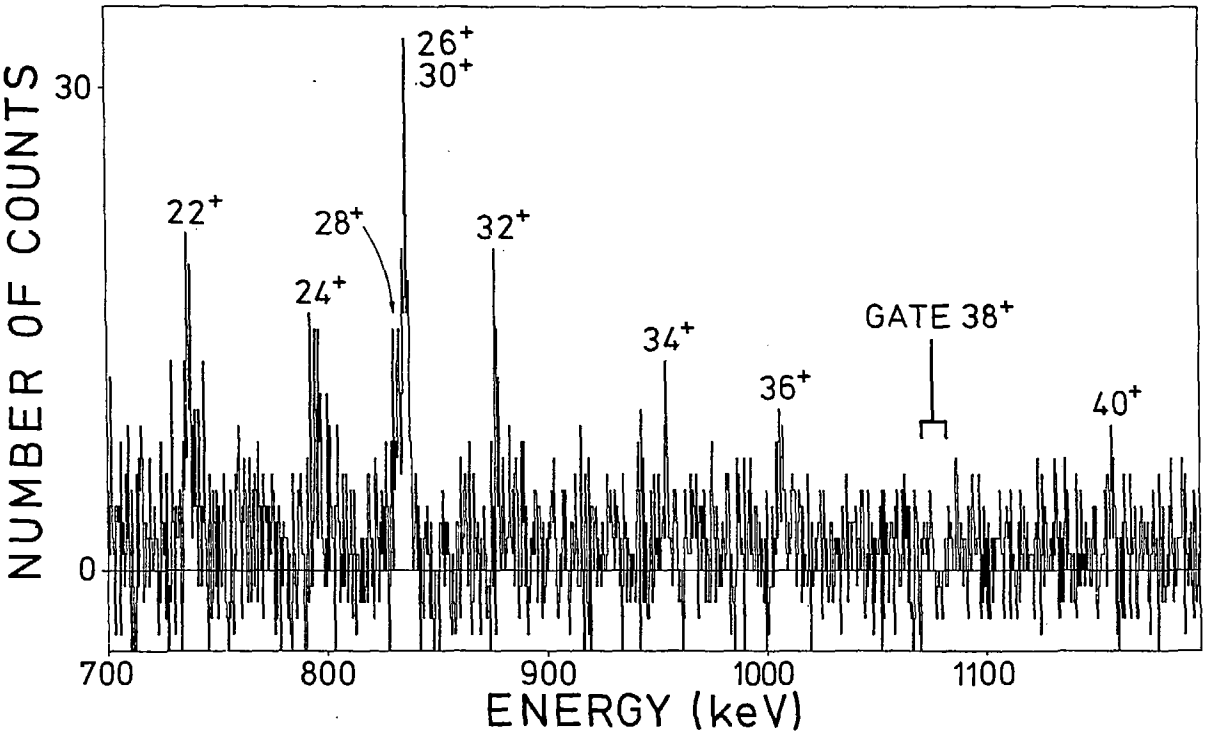
NUMBER OF COUNTS
30
0
22+
24+
28+
26+
30+
32+
34+
36+
GATE 38+
40+
700
800
900
1000
1100
ENERGY (keV)

Fig. 7 b

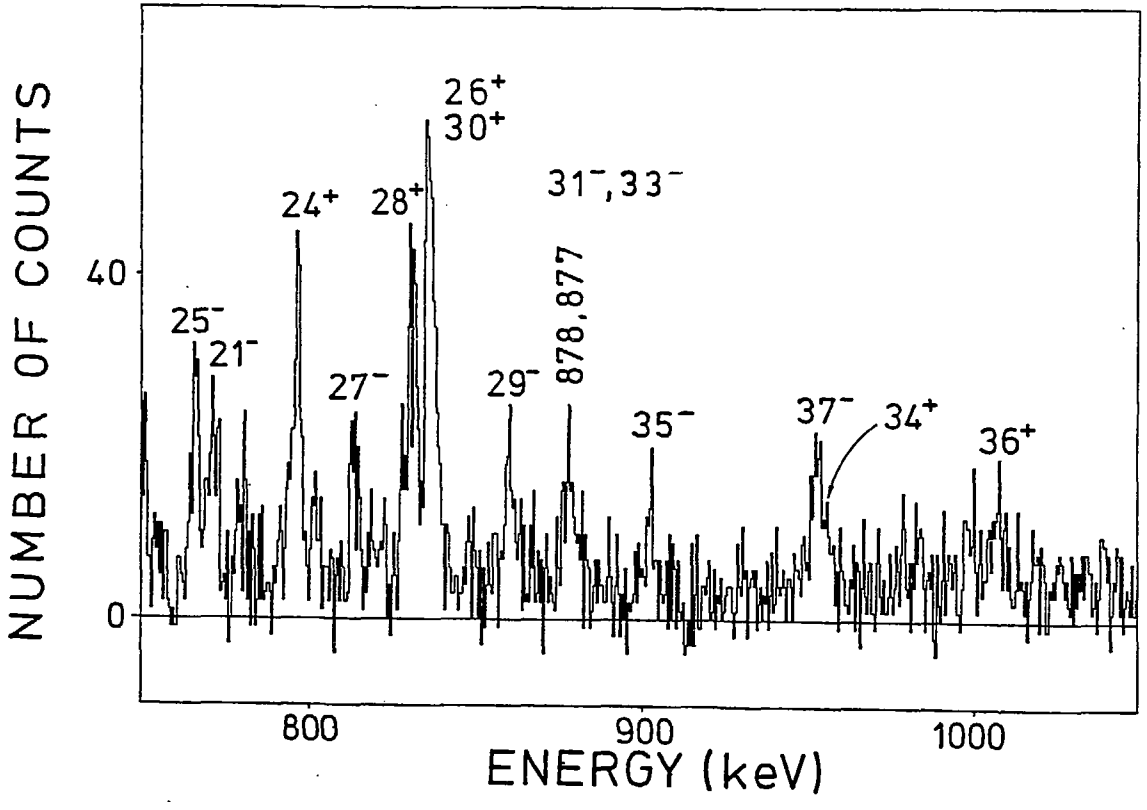
NUMBER OF COUNTS
40
0
25⁻
21⁻
24⁺
27⁻
28⁺
26⁺
30⁺
29⁻
878,877
31⁻,33⁻
35⁻
37⁻
34⁺
36⁺
800
900
1000
ENERGY (keV)

Fig. 7 c

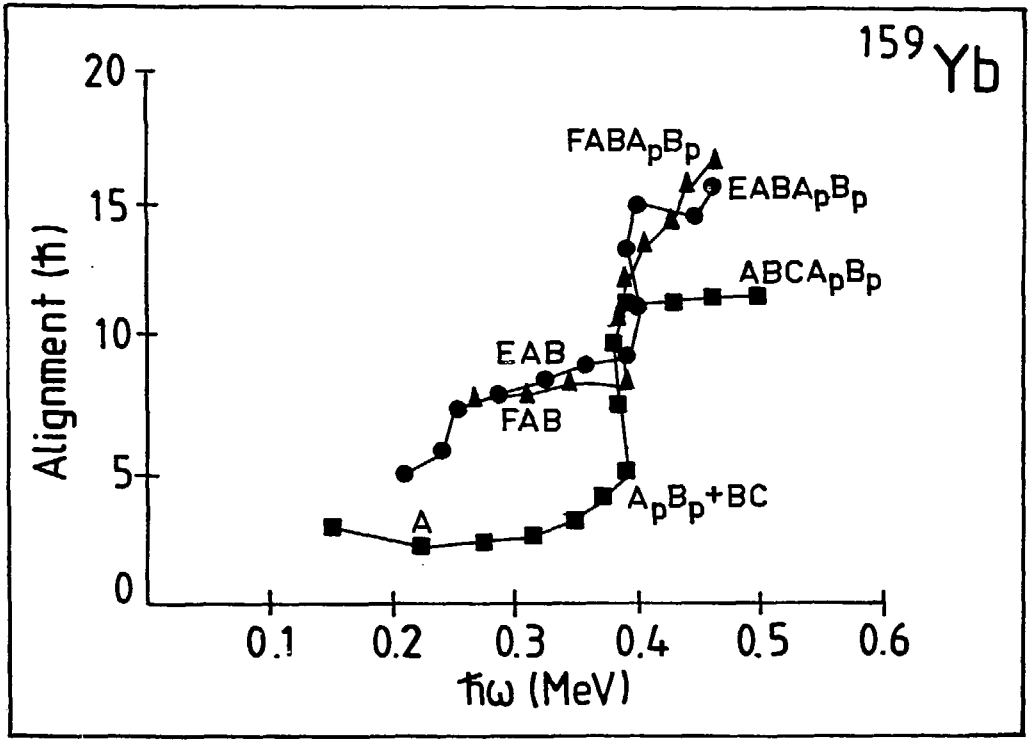
159Yb
20
15
10
5
0
Alignment (ħ)
FABA$_p$B$_p$
EABA$_p$B$_p$
ABCA$_p$B$_p$
EAB
FAB
A
A$_p$B$_p$+BC
0.1
0.2
0.3
0.4
0.5
0.6
ħω (MeV)

Fig. 8 a

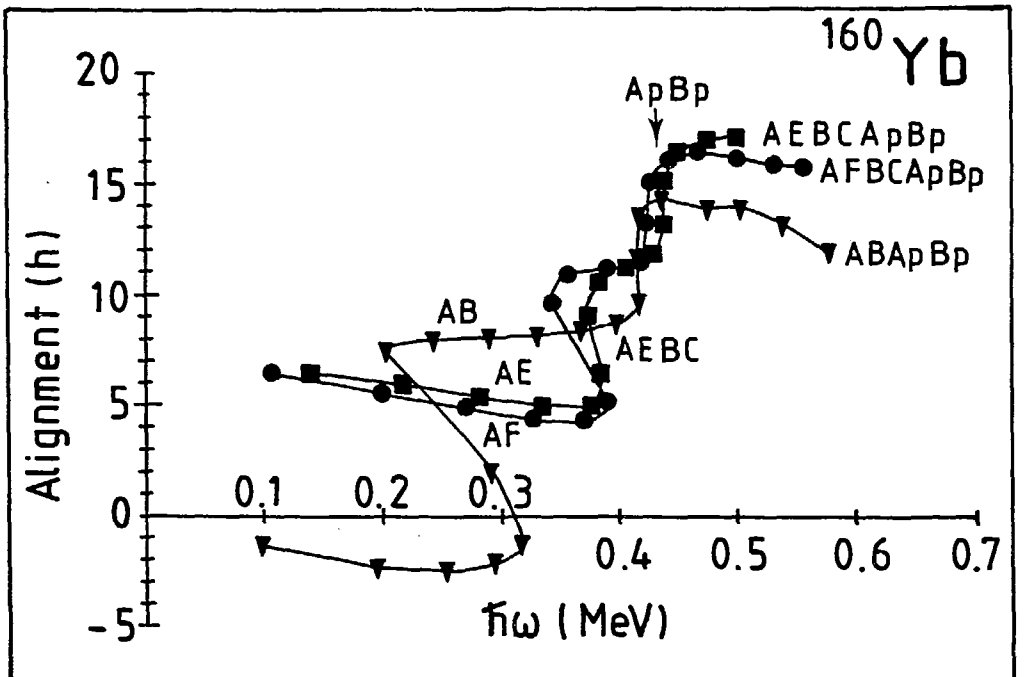
160 Yb
ApBp
AEBCApBp
AFBCApBp
ABApBp
AB
AEBC
AE
AF
Alignment (h)
20
15
10
5
0
-5
0.1
0.2
0.3
0.4
0.5
0.6
0.7
ħω (MeV)

Fig. 8 b

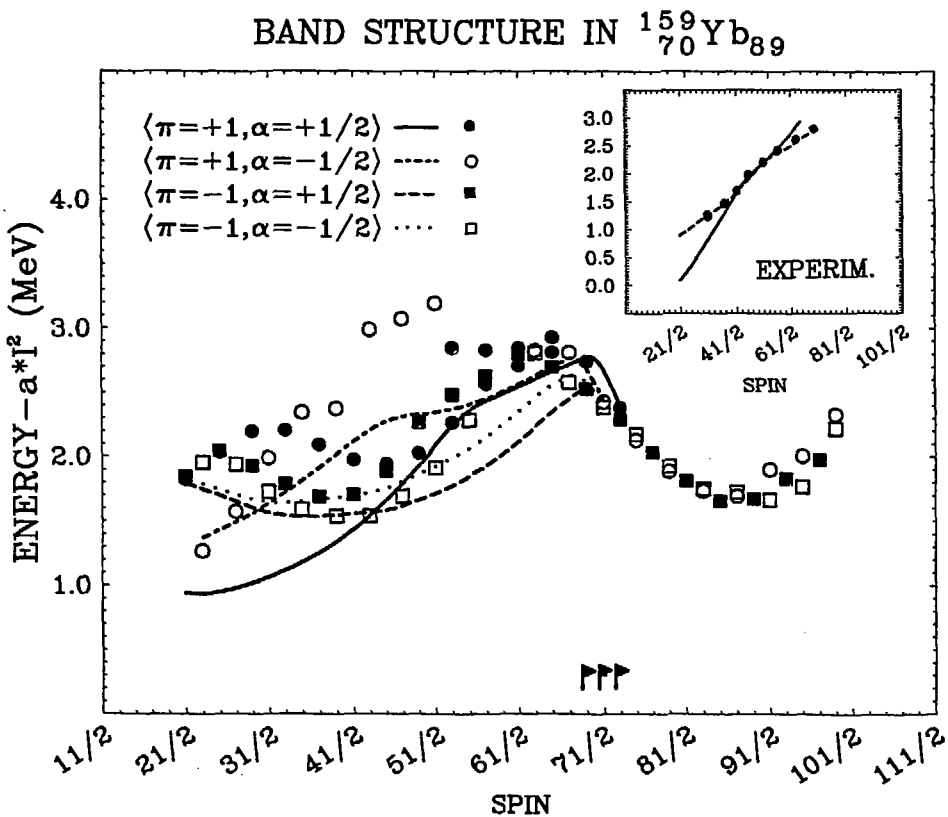
BAND STRUCTURE IN $^{159}_{70}Yb_{89}$
⟨π=+1,α=+1/2⟩
⟨π=+1,α=−1/2⟩
⟨π=−1,α=+1/2⟩
⟨π=−1,α=−1/2⟩
EXPERIM.
SPIN
ENERGY−a*I² (MeV)
4.0
3.0
2.0
1.0
11/2
21/2
31/2
41/2
51/2
61/2
71/2
81/2
91/2
101/2
111/2
SPIN

Fig. 9

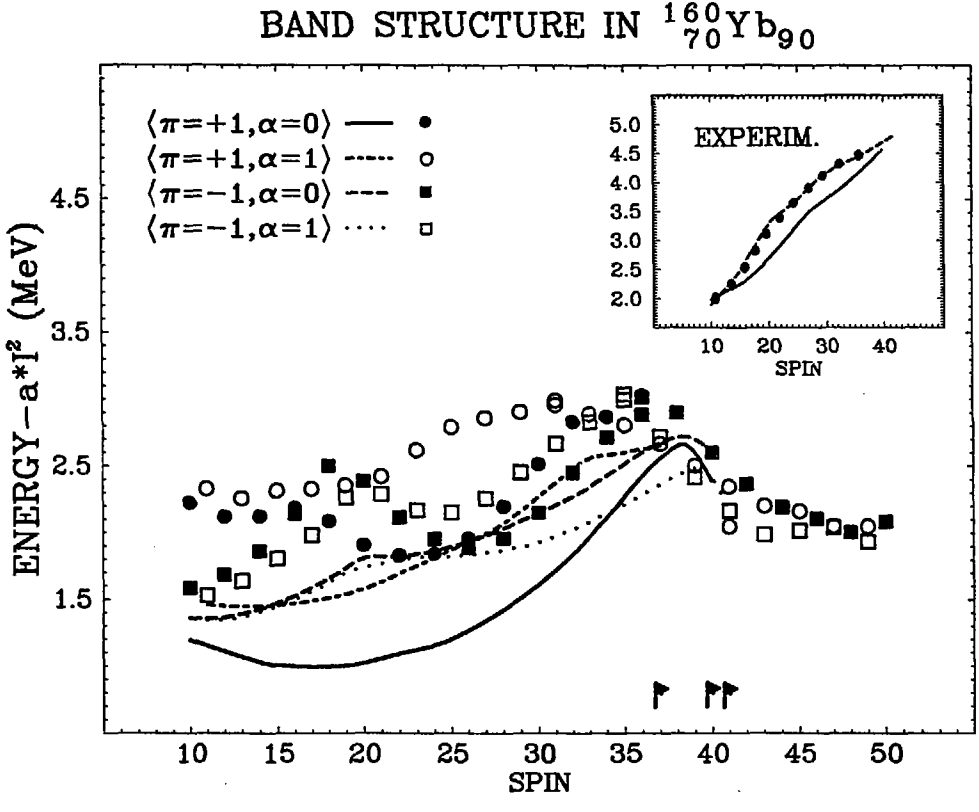
BAND STRUCTURE IN $^{160}_{70}Yb_{90}$
⟨π=+1,α=0⟩
⟨π=+1,α=1⟩
⟨π=−1,α=0⟩
⟨π=−1,α=1⟩
EXPERIM.
5.0
4.5
4.0
3.5
3.0
2.5
2.0
10
20
30
40
SPIN
ENERGY−a*I² (MeV)
4.5
3.5
2.5
1.5
10
15
20
25
30
35
40
45
50
SPIN

Fig. 10

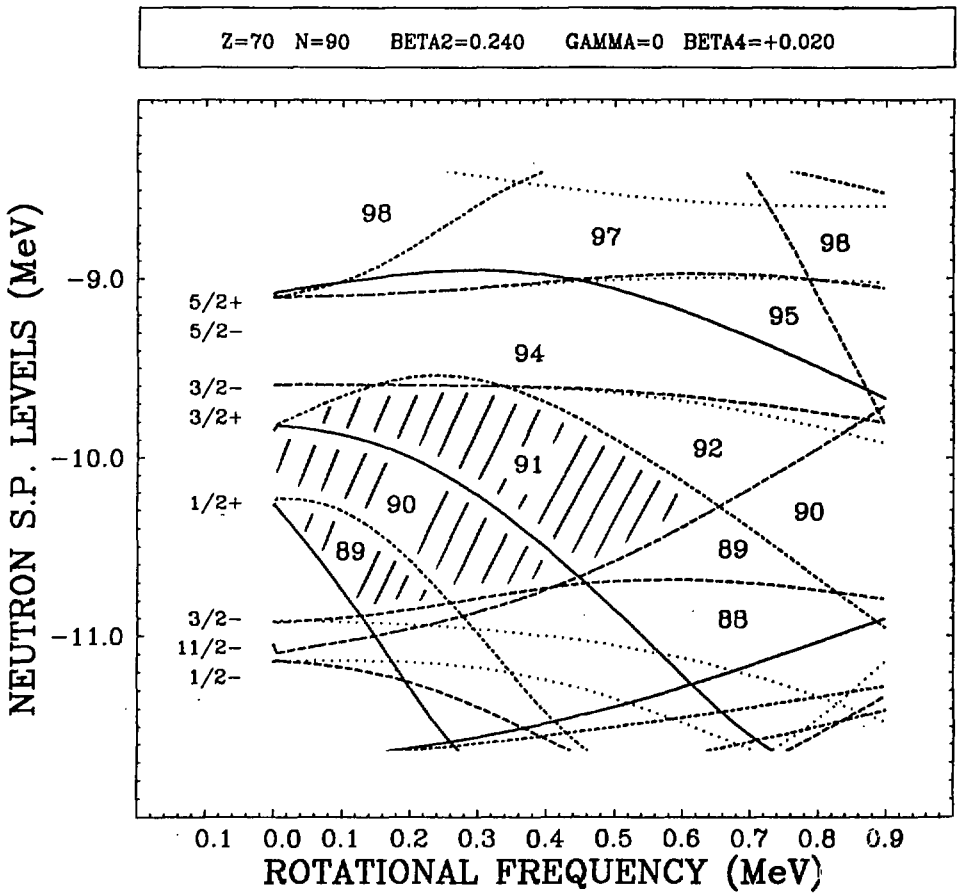
Z=70 N=90 BETA2=0.240 GAMMA=0 BETA4=+0.020
NEUTRON S.P. LEVELS (MeV)
-9.0
-10.0
-11.0
5/2+
5/2-
3/2-
3/2+
1/2+
3/2-
11/2-
1/2-
98
97
98
95
94
92
91
90
90
89
89
88
0.1 0.0 0.1 0.2 0.3 0.4 0.5 0.6 0.7 0.8 0.9
ROTATIONAL FREQUENCY (MeV)

Fig. 11 a

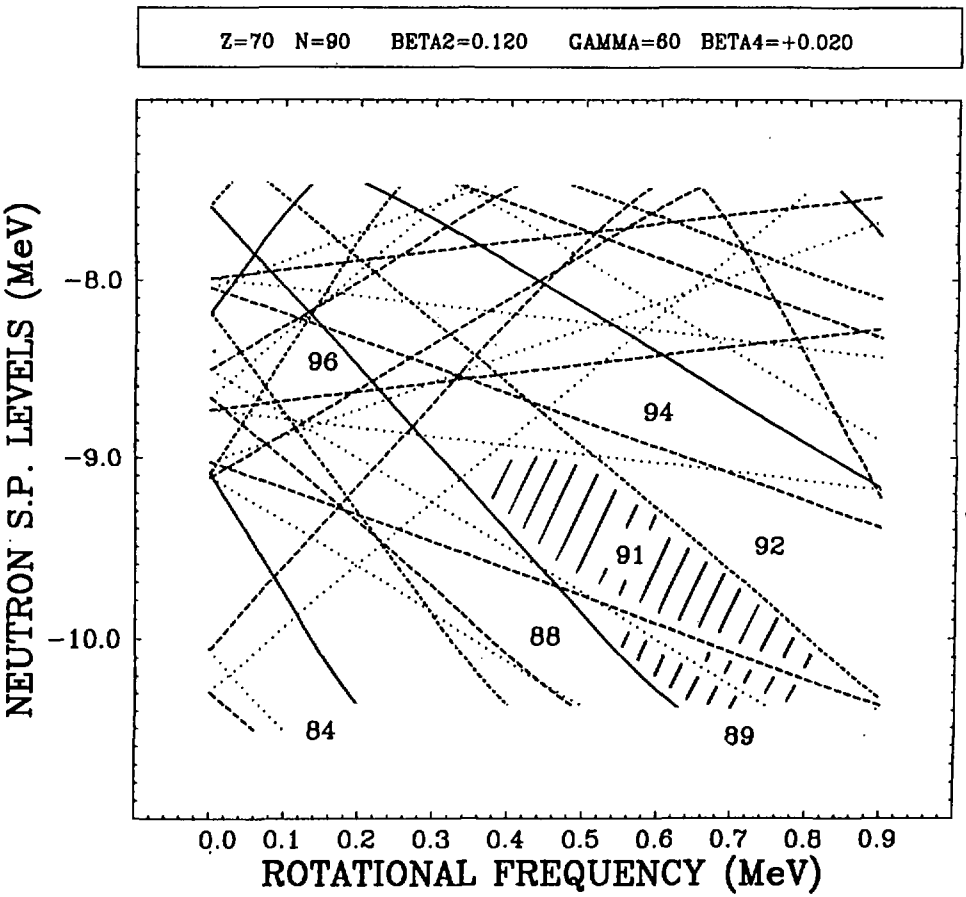
Z=70 N=90 BETA2=0.120 GAMMA=60 BETA4=+0.020
NEUTRON S.P. LEVELS (MeV)
-8.0
-9.0
-10.0
96
94
92
91
88
84
89
0.0 0.1 0.2 0.3 0.4 0.5 0.6 0.7 0.8 0.9
ROTATIONAL FREQUENCY (MeV)

Fig. 11 b

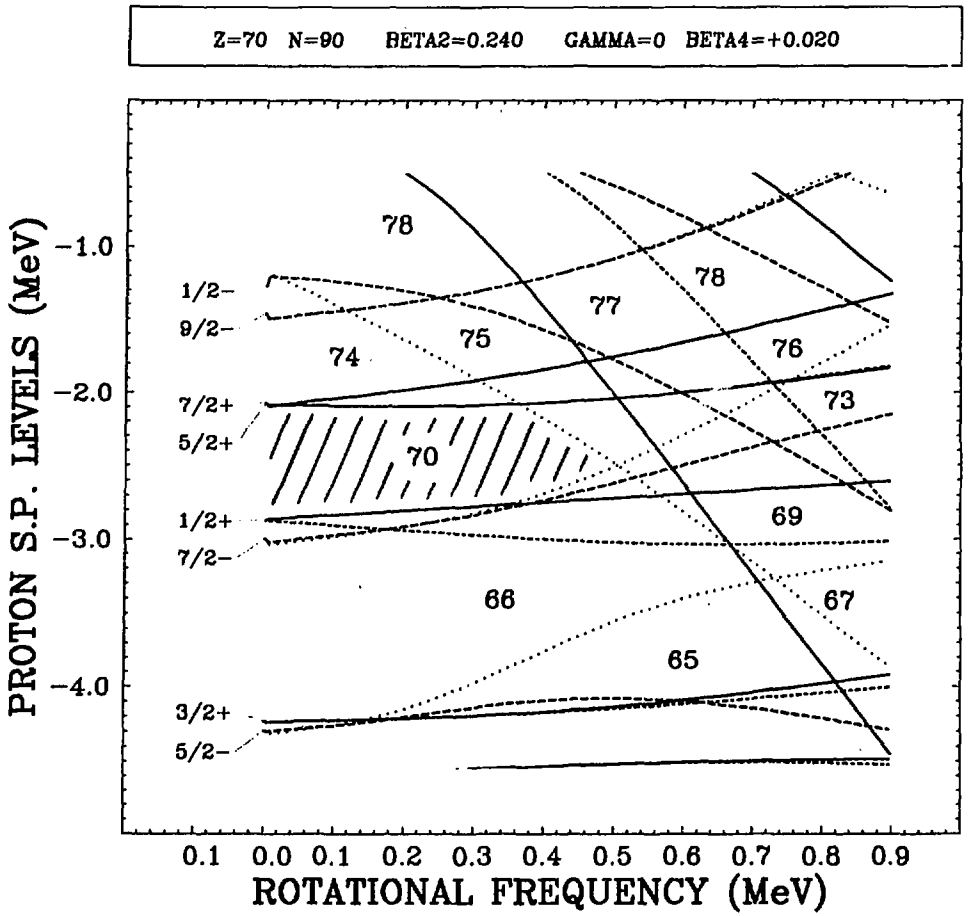
Z=70 N=90 BETA2=0.240 GAMMA=0 BETA4=+0.020
PROTON S.P. LEVELS (MeV)
−1.0
−2.0
−3.0
−4.0
1/2−
9/2−
7/2+
5/2+
1/2+
7/2−
3/2+
5/2−
78
78
77
74
75
76
73
70
69
66
67
65
0.1 0.0 0.1 0.2 0.3 0.4 0.5 0.6 0.7 0.8 0.9
ROTATIONAL FREQUENCY (MeV)

Fig. 12 a

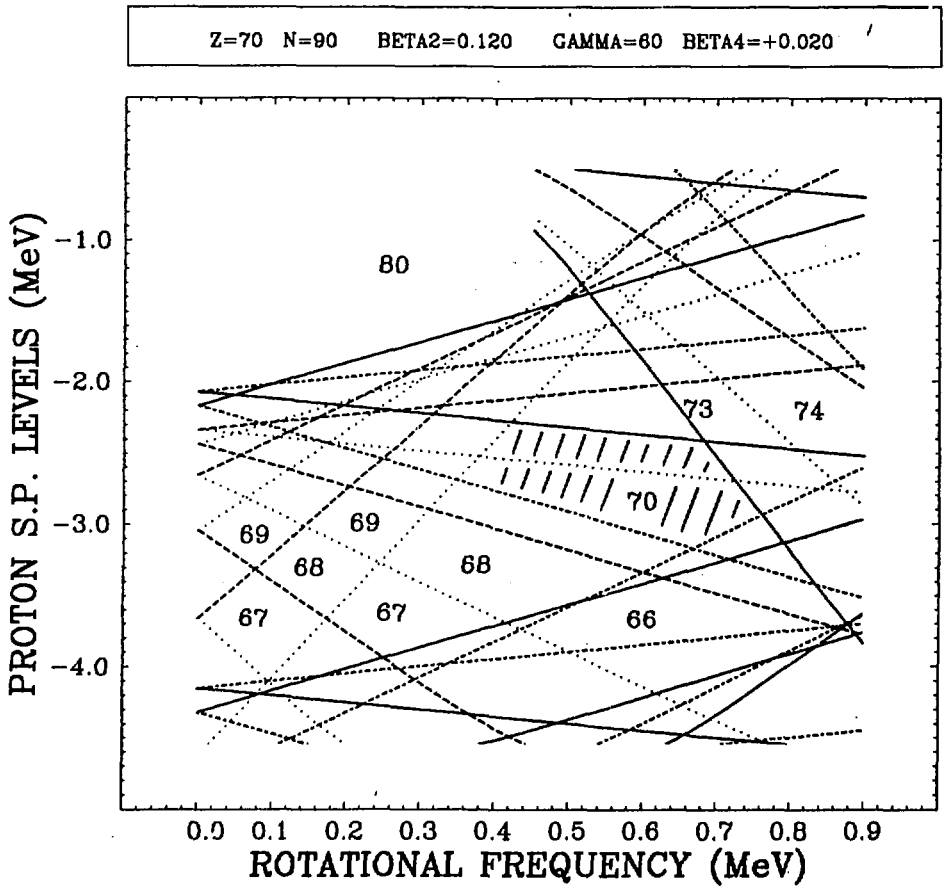
Z=70 N=90 BETA2=0.120 GAMMA=60 BETA4=+0.020
PROTON S.P. LEVELS (MeV)
-1.0
-2.0
-3.0
-4.0
80
73
74
70
69
69
68
68
67
67
66
0.0 0.1 0.2 0.3 0.4 0.5 0.6 0.7 0.8 0.9
ROTATIONAL FREQUENCY (MeV)

Fig. 12 b

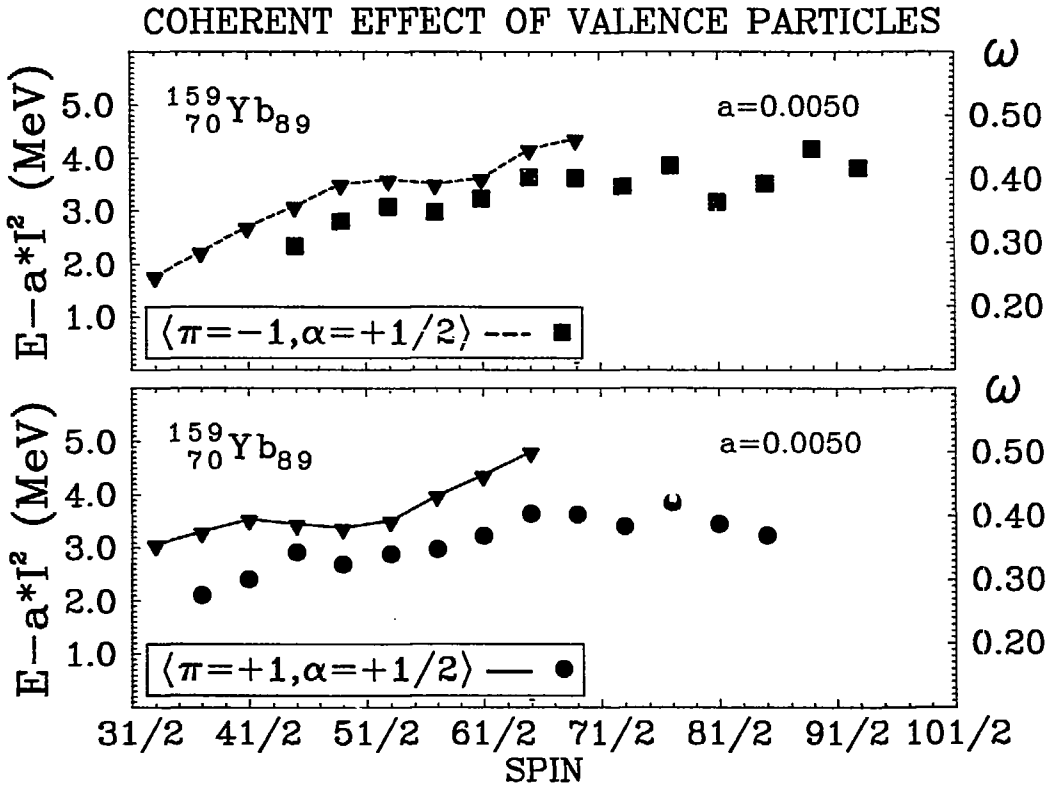
COHERENT EFFECT OF VALENCE PARTICLES
$^{159}_{70}Yb_{89}$
a=0.0050
ω
0.50
0.40
0.30
0.20
E−a*I² (MeV)
5.0
4.0
3.0
2.0
1.0
⟨π=−1,α=+1/2⟩ --- ■
$^{159}_{70}Yb_{89}$
a=0.0050
⟨π=+1,α=+1/2⟩ — ●
31/2 41/2 51/2 61/2 71/2 81/2 91/2 101/2
SPIN

Fig. 13

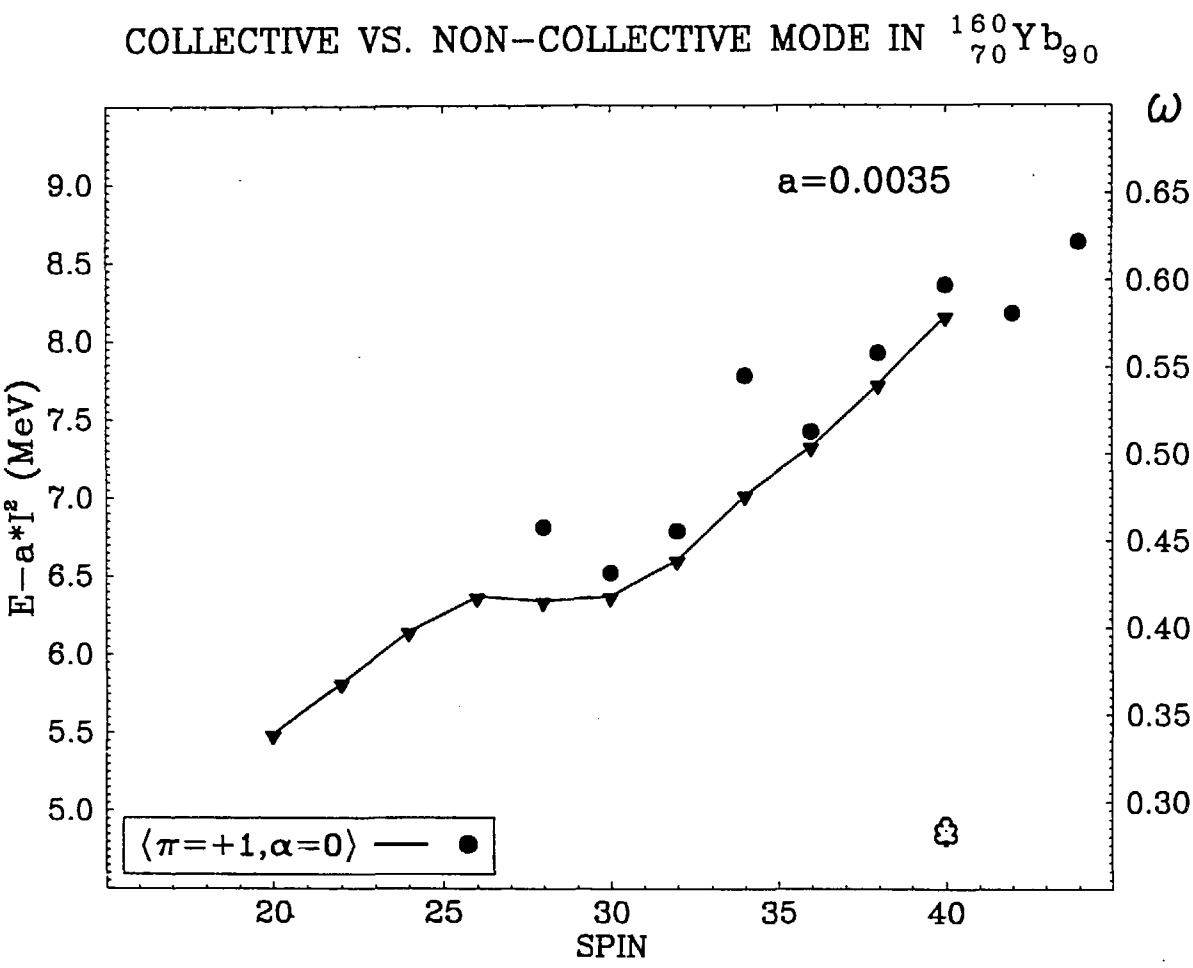
COLLECTIVE VS. NON-COLLECTIVE MODE IN $^{160}_{70}Yb_{90}$
ω
a=0.0035
E−a*I² (MeV)
9.0
8.5
8.0
7.5
7.0
6.5
6.0
5.5
5.0
0.65
0.60
0.55
0.50
0.45
0.40
0.35
0.30
⟨π=+1,α=0⟩
20
25
30
35
40
SPIN

Fig. 14

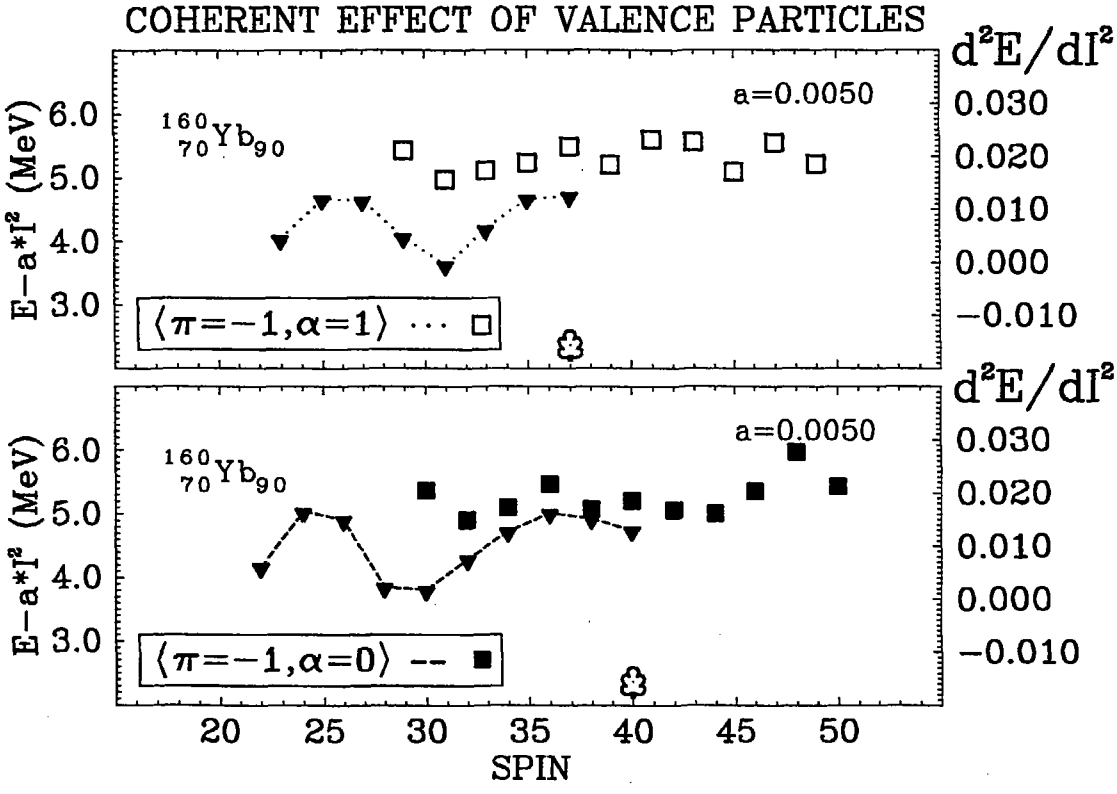
COHERENT EFFECT OF VALENCE PARTICLES
d^2E/dI^2
a=0.0050
$^{160}_{70}Yb_{90}$
E−a*I² (MeV)
6.0
5.0
4.0
3.0
0.030
0.020
0.010
0.000
−0.010
⟨π=−1,α=1⟩ ··· □
⟨π=−1,α=0⟩ -- ■
20
25
30
35
40
45
50
SPIN

Fig. 15

Imprimé
au Centre de
Recherches Nucléaires
Strasbourg
1987